



Review

Networking Strategies of Triboelectric Nanogenerators for Harvesting Ocean Blue Energy

Xianye Li^{1,2}, Liang Xu^{1,2,*}  and Zhong Lin Wang^{1,2,3,*}

¹ Beijing Institute of Nanoenergy and Nanosystems, Chinese Academy of Sciences, Beijing 101400, China
² School of Nanoscience and Engineering, University of Chinese Academy of Sciences, Beijing 100049, China
³ Georgia Institute of Technology, Atlanta, GA 30332-0245, USA
* Correspondence: xuliang@binn.cas.cn (L.X.); zlwang@gatech.edu (Z.L.W.)

Abstract: The utilization of abundant blue energy in the ocean could greatly contribute to achieving carbon neutrality. However, the unsolved economic and technical challenges of traditional technologies for harvesting blue energy have resulted in slow progress. Triboelectric nanogenerators (TENGs), as a new approach for converting mechanical energy into electricity, have great potential for blue energy harvesting, which can be connected as networks with different numbers of units for varying scales of energy harvesting. Here, recent advances of networking strategies of TENGs for harvesting blue energy are reviewed, mainly concerning mechanical and electrical connection designs. Anchoring strategies of devices and networks are also discussed. The development of TENG networks could provide an effective solution for large-scale ocean blue energy harvesting, which can also serve as an in-situ energy station or power source for self-powered systems, supporting various marine equipment and activities.

Keywords: triboelectric nanogenerator; network; blue energy; wave energy; energy harvesting



Citation: Li, X.; Xu, L.; Wang, Z.L. Networking Strategies of Triboelectric Nanogenerators for Harvesting Ocean Blue Energy. *Nanoenergy Adv.* **2024**, *4*, 70–96. <https://doi.org/10.3390/nanoenergyadv4010004>

Academic Editor: Joao Ventura

Received: 2 November 2023

Revised: 3 January 2024

Accepted: 16 January 2024

Published: 22 January 2024



Copyright: © 2024 by the authors. Licensee MDPI, Basel, Switzerland. This article is an open access article distributed under the terms and conditions of the Creative Commons Attribution (CC BY) license (<https://creativecommons.org/licenses/by/4.0/>).

1. Introduction

As the frequency of extreme climate events rises, the global call for carbon neutrality resonates louder than ever, urging humanity to seek innovative solutions that transcend traditional energy paradigms. The optimization of energy structure through the utilization of clean energy constitutes a pivotal pathway. Covering more than 70% of the earth's surface, the ocean not only serves as a treasury of life but also contains vast reserves of clean energy, regarded as blue energy [1–3]. Developing and harnessing blue energy will accommodate the ever-growing demand for onshore energy [4]. Meanwhile, as human exploration of the ocean advances, the growing demand for a sustainable power supply of equipment deployed in offshore and deep-sea areas is looking for solutions from in-situ blue energy resources.

Blue energy exists in five typical forms: wave energy, tidal energy, current energy, thermal energy, and osmotic energy. Among them, wave energy, consisting of wave potentials and kinetic energy, is the most focused, which is characterized by its widespread distribution, easy accessibility, and abundant reserves [5,6]. As a typical form of blue energy, wave energy has garnered increasing attention over the past few decades. However, with the complex marine environment and low energy density, it faces dual challenges in terms of the technology and economics required for commercial harvesting. Specifically, wave energy exhibits multiple amplitudes, low and erratic frequencies, and varying directions, making it challenging for the traditional method based on the electromagnetic generator (EMG) to achieve high conversion efficiency directly [7]. Consequently, additional bulky and complex structures are often required to improve its performance. Moreover, the harsh marine environment reduces the reliability and increases the maintenance costs of such devices.

The triboelectric nanogenerator (TENG), first invented in 2012, emerges as a promising technology for converting mechanical energy into electricity [8,9]. This innovative device works based on the coupling of triboelectrification and electrostatic induction [10–12]. Exhibiting notable merits, including structural flexibility, facile fabrication, and versatile material choices [13–15], TENGs show great potential for wave energy harvesting [9], as well as some other forms of blue energy. In comparison to the bulky and complex devices mentioned above, TENGs possess several advantages. Firstly, TENGs demonstrate good responses to disordered water waves. Through thoughtful structural design, TENGs can directly generate outputs with a relatively high voltage and low current from low-frequency and multiple-amplitude waves, eliminating the need for additional mechanical mechanisms. Secondly, the relatively simple structure and fabrication process of TENGs contribute to their cost-effectiveness, making it a viable option for wave energy harvesting from an economic perspective. Lastly, miniaturized TENG units can be organized into modules and networks of various scales according to energy requirements. This not only reflects their inherent flexibility, allowing for their adaptability to varied scenarios, but also mitigates maintenance costs as the malfunction of single units does not propagate through the network [6,16,17].

The TENG network typically has a hierarchical architecture, consisting of multiple modules, each of which contains a number of TENG units. Such units need to be connected both mechanically and electrically as a network. Effective networking strategies can ensure the total performance of a large number of units, which is vital for blue energy harvesting. In terms of mechanical connections, the basic function is to realize the integrity of the network. Furthermore, for enhancing the performance through networking, investigating its impact on the output of individual units, the interaction between waves and the network, and the energy transfer within the network becomes crucial. Meanwhile, the local anchoring strategy for units or networks (ultimately anchored on the seabed) varies depending on the excitation method of the device or network, which is also essential for their deployment. Electrical connections focus on how the energy output of units within the network is merged, addressing specific aspects such as maximizing output, balancing cable loss and cost, and mitigating environmental impacts. Combined with proper power management, TENG networks can supply electricity for a wide variety of devices and engineering applications.

In this paper, recent advances of networking strategies of TENGs for harvesting blue energy are reviewed. This review mainly concerns the designs of mechanical and electrical connections, including simple aggregation with weak coupling, strongly coupled networks, dynamic self-assembly networks, chiral networks, and three-dimensional networks for the mechanical connection; rectification and power management, networking topology and cable loss, and multifunctional design for the electrical connection. The designs of these networking strategies have resulted in an enhanced performance in the conversion of blue energy through TENG networks. Anchoring strategies of devices and networks are also discussed. Finally, the future challenges of networking strategies of TENGs and the outlook of blue energy harvesting are discussed.

2. Triboelectric Nanogenerator Networks for Blue Energy

2.1. Working Principle of Triboelectric Nanogenerators

The TENGs convert mechanical energy into electricity through the coupling of triboelectrification and electrostatic induction, classified into five working modes: contact-separation mode, lateral-sliding mode, single-electrode mode, free-standing mode, and rolling mode (Figure 1a–e) [9,11,18].

As shown in Figure 1a, the contact-separation mode of TENGs operates through the physical contact of two dielectric surfaces, which possess distinct capabilities for attracting electrons. The contact process generates opposite triboelectric charges on the two surfaces due to contact electrification. When the surfaces separate with a gap, a potential drop is created between the electrodes on the backside of the dielectric layers, which drives the electrons from one electrode to the other through the external load. In the process of contact,

the accompanied potential change will drive the electrons to flow back. Periodic contact and separation movements will drive the electrons to move back and forth between the electrodes, generating an alternate current (AC) output in the external circuit [19].

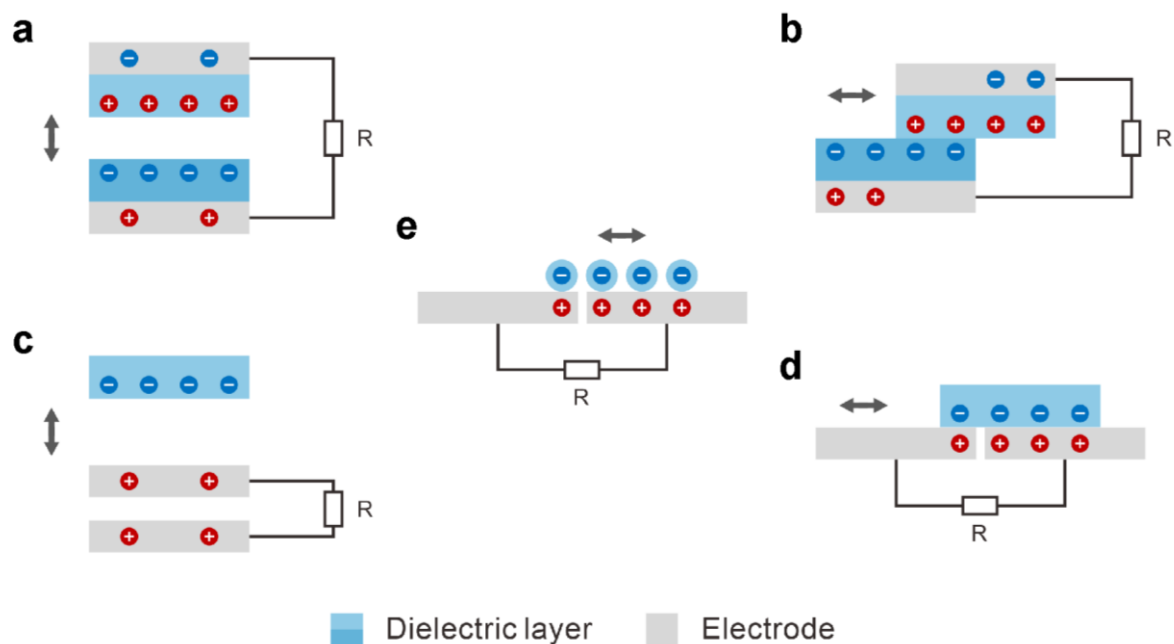


Figure 1. Five working modes of TENGs. (a) Contact-separation mode. (b) Lateral-sliding mode. (c) Single-electrode mode. (d) Free-standing mode. (e) Rolling mode.

The lateral-sliding mode of TENGs, as shown in Figure 1b, is based on the sliding motion of two dielectric surfaces. Static charges are generated after the contact of two dielectric surfaces. When the surfaces are in complete contact, the positive and negative charges are quite close, resulting in almost no potential difference between the electrodes. As the dielectric layers relatively slide parallel to the interface, the exposed charges lead to a potential difference that drives the electrons to flow between the electrodes through the external circuit [20].

For the single-electrode mode shown in Figure 1c, the moving dielectric layer is unrestricted by electrodes or wires. One electrode is set to contact with the dielectric layer, while another electrode, serving as the reference electrode, can be placed arbitrarily or replaced by the ground, resulting in only one electrode in the device. After the triboelectrification of the two surfaces, the electrical potential variation due to relative motion is balanced by the induced current flow through the circuit. Although the charge transfer efficiency of the single-electrode mode is limited by electrostatic shielding, it finds extensive application in harvesting energy from freely moving objects [21].

In the free-standing mode of TENGs (Figure 1d), there is also a freely moving dielectric layer. When the charged dielectric layer, due to triboelectrification, moves on a pair of electrodes, the electrodes will exhibit varying potentials, which result in the flow of electrons between the electrodes to balance the local potential distribution. Based on this principle, the motion of the dielectric layer induces the current flow in the external circuit, forming an AC output [22].

The rolling mode of TENGs, as shown in Figure 1e, is based on the rolling triboelectrification between the spheres and the surface. The rolling of the spheres over a pair of electrodes changes the potentials in the electrodes, driving charges to move through the external circuit to reestablish balance. The rolling mode of TENGs efficiently reduces material wear while maintaining high output [18].

2.2. General Network Architecture

For large-scale blue energy harvesting, typically, networks consisting of a large number of TENG units need to be constructed, as shown in Figure 2a. The network based on a hierarchical architecture comprises multiple modules, each composed of TENG units. The working mechanism of a typical rolling ball structure unit is illustrated in Figure 2b. Under the agitation of water waves, a dielectric ball rolls inside a sphere made of another dielectric material, generating opposite triboelectric charges on both surfaces. Meanwhile, the induced charges on the back electrodes flow through the external load to balance the potential difference caused by the dielectric ball. This device structure exhibits a good response to low-amplitude and multi-directional water waves.

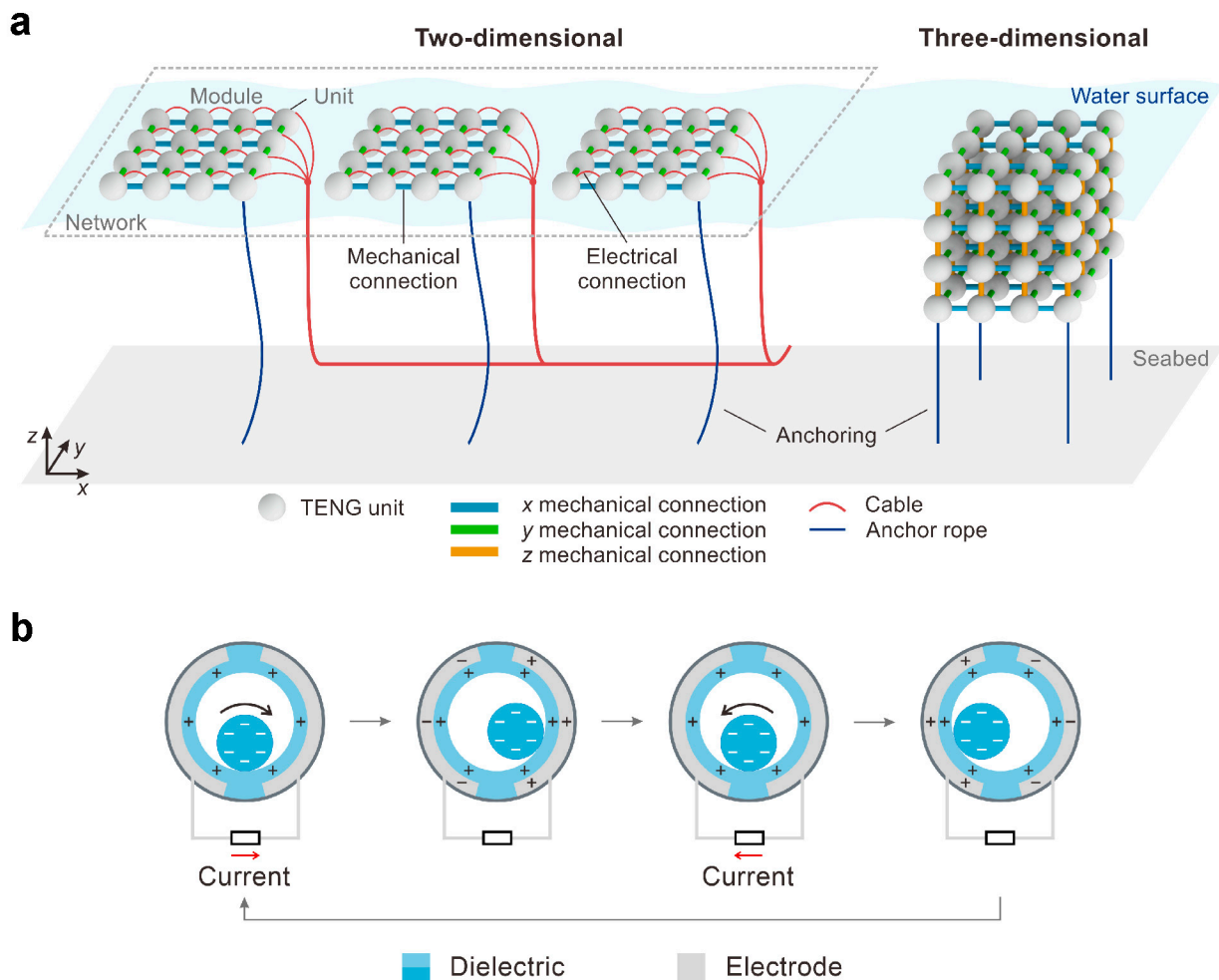


Figure 2. General network architecture and the working mechanism of TENG units. (a) General network architecture for harvesting blue energy. (b) The working mechanism of a typical rolling ball structure TENG unit.

The networking strategy of the units primarily focuses on the mechanical and electrical connections, as shown in Figure 2a. Mechanical connections realize the integrity of the network. Simultaneously, the network's topology determines the interconnected relationship of the units, typically forming a square grid. Additionally, the stiffness of the connections and connection methods are crucial for the coupling of unit outputs and the behavior of energy transfer within the network. The network can be configured as a two-dimensional network distributed along the water surface through mechanical connections in the x and y directions. Alternatively, the network can be extended below the water surface to form a three-dimensional network by adding connections in the z direction. Networks are typically anchored on the seabed, serving the dual purposes of fixing the distribution position and

aligning with the excitation mode of the network. Electrical connections focus on how to merge the energy output of units within the network, addressing specific aspects such as maximizing output, balancing cable loss and costs, and mitigating environmental impacts. This review mainly concerns designs of mechanical and electrical connections. Furthermore, anchoring strategies of devices and networks are also discussed.

2.3. Typical Triboelectric Nanogenerator Units

TENG units are the foundational components of the network for harvesting blue energy. The design of TENG units should address challenges such as efficient power-take-off (PTO) from low-frequency water waves and effectively converting input mechanical energy into electricity. Here, typical TENG unit designs are presented briefly, including rolling ball structure, multilayer structure, spring-oscillator structure, pendulum and grating structure, and liquid-solid contact structure.

The rolling ball structure represents the most typical design for TENG units adopted in harvesting wave energy. Wang et al. first proposed a device based on the free-standing mode with a rolling ball structure, ensuring the durability of the device [23]. As shown in Figure 3a, the device utilizes nylon or polytetrafluoroethylene (PTFE) as the dielectric material for the ball, resulting in a charge output of 24 nC. Xu et al. introduced an optimization strategy for the free-standing mode device by employing silicon rubber after ultraviolet (UV) treatment as the dielectric material for the ball (Figure 3b) [24]. Additionally, small particles are mixed into the silicone rubber inside the shell. These enhancements increase the contact area of the device and improve adhesive issues, resulting in an increased charge output of approximately 70 nC, and the device exhibits responsiveness to weak agitation with a 5 mm amplitude. Considering the limited contact area of a single ball inside the device, Yang et al. designed a three-dimensional (3D) electrode device with multiple pellets [25]. This device comprises a pair of multi-channel 3D electrodes and fluorinated ethylene propylene (FEP) pellets filling the channels (Figure 3c). In this design, the contact area is significantly increased, leading to a further improvement in the charge output, reaching about 0.5 μC . Furthermore, with the flexibility in the design of the electrodes and channels, this structure can be further modified into different shapes to adapt to various internal spaces.

Generally, TENGs function based on the contact area, which significantly determines the output charge and power density in a limited space. A multilayer structure is an effective strategy, typically based on the contact-separation mode, to increase the contact area. Xu et al. were the first to apply a multilayer structure to wave energy harvesting devices [26]. As shown in Figure 3d, the device adopts a flexible thin film as the substrate for sub-units, combined with a PTFE dielectric layer and Cu, Al electrodes to form a contact-separation mode TENG. By designing two independent air chambers and utilizing the changes in the chamber air pressure, the sub-units are driven to contact or separate fully and nearly synchronously. In such a device, each sub-unit can output transferred charges of about 0.22 μC . With the integration of 38 sub-units, the single-cycle rectified output charge can reach 15 μC .

The spring-oscillator structure is a design that leverages the energy storage capability of a spring system to enhance the device's response to water waves. After the device is agitated by water waves, a portion of the mechanical energy is stored in the spring system. When the TENG is insufficient to completely convert the mechanical energy into electricity within a single cycle, the energy stored in the spring will be gradually released in a damped oscillation state of multiple cycles. The dynamic model of the system can be simplified as a resonator composed of a mass block and a spring. The multilayer structure device designed by Xu et al. mentioned above incorporates the spring-oscillator structure coupled with wave agitation (Figure 3e) [26]. The oscillator is agitated to oscillate under vertical wave excitation, and the upper and lower air chambers periodically collide with the shell, thereby altering the air pressure and driving the TENG sub-units. Under pulse excitation,

the device induces a series of internal oscillations related to the inherent frequency of the oscillator, extending the output duration, as shown in Figure 3f.

The pendulum structure features a swinging mass, which shows oscillating behavior of the conversion between gravitational potential energy and kinetic energy. Similar to the spring-oscillator structure, pulse or step excitation can induce the device to oscillate at its inherent frequency, entering an oscillating state even under low-frequency water wave agitation. The grating structure is a typical design for high-performance TENGs, converting low-frequency excitation into high-frequency electrical output through periodic grating electrodes. Furthermore, grating structure devices exhibit scalability and can easily be expanded into array structures to further enhance device output. Figure 3g demonstrates a high-performance device of a pendulum structure combined with a grating structure [27]. A set of stators is fixed on a cylindrical shell, and a set of rotators is connected to a pendulum through a shaft and mounted on the shell via bearings. Upon water wave agitations, the pendulum swings inside the device, driving the rotation of the rotators. As shown in Figure 3h, Lin et al. reported a pendulum structure device consisting of three parts: an electrode layer, a pendulum triboelectric layer, and thin stripes [28]. The designs of the gap, which is between the pendulum triboelectric layer and the electrode layer, and thin PTFE stripes operate in a non-contact state at small swing angles. When the swing angle is large enough, soft contact is realized to enhance triboelectric charges on the pendulum surface. Based on this design, the device is easily agitated, leading to an extended duration of oscillation. Zhang et al. proposed an active resonance TENG with a combination of the pendulum and multilayer structures, which consists of a pendulum, a tumbler, and a flexible ring TENG (Figure 3i) [29]. A high-frequency output is generated under low-frequency non-harmonic excitation due to the oscillations of the simple pendulum and tumbler.

The liquid-solid contact structure is based on the triboelectrification between the liquid and solid surfaces. After the electrification process, the liquid's behavior on the dielectric layer's surface leads to changes in the charge screening state, generating charge outputs in the external circuit based on electrostatic induction. Zhu et al. first proposed a device that utilizes the sliding motions of water on a hydrophobic surface to harvest wave energy [30]. The working principle of this device is depicted in Figure 3j. This type of devices typically requires the existence of the gas phase to separate the liquid and solid phases, which is generally set on the water surface. Qin et al. designed a device that works without a gas phase and can even function directly underwater by introducing an oil phase in the structure [31]. This device's structure is shown in Figure 3k. Unlike traditional TENGs, this device exploits the electric double layer (EDL) capacitance formed at the liquid-solid interface. In a water environment, by squeezing oil droplets on the dielectric surface, the expansion of the oil droplets and the movement of the oil-water-solid three-phase line can be observed, leading to charge transfer in the back electrode. This charge transfer is primarily attributed to the difference in the EDLs at the water-solid and oil-solid interfaces, with the oil phase sweeping away ions near the dielectric surface in the EDL.

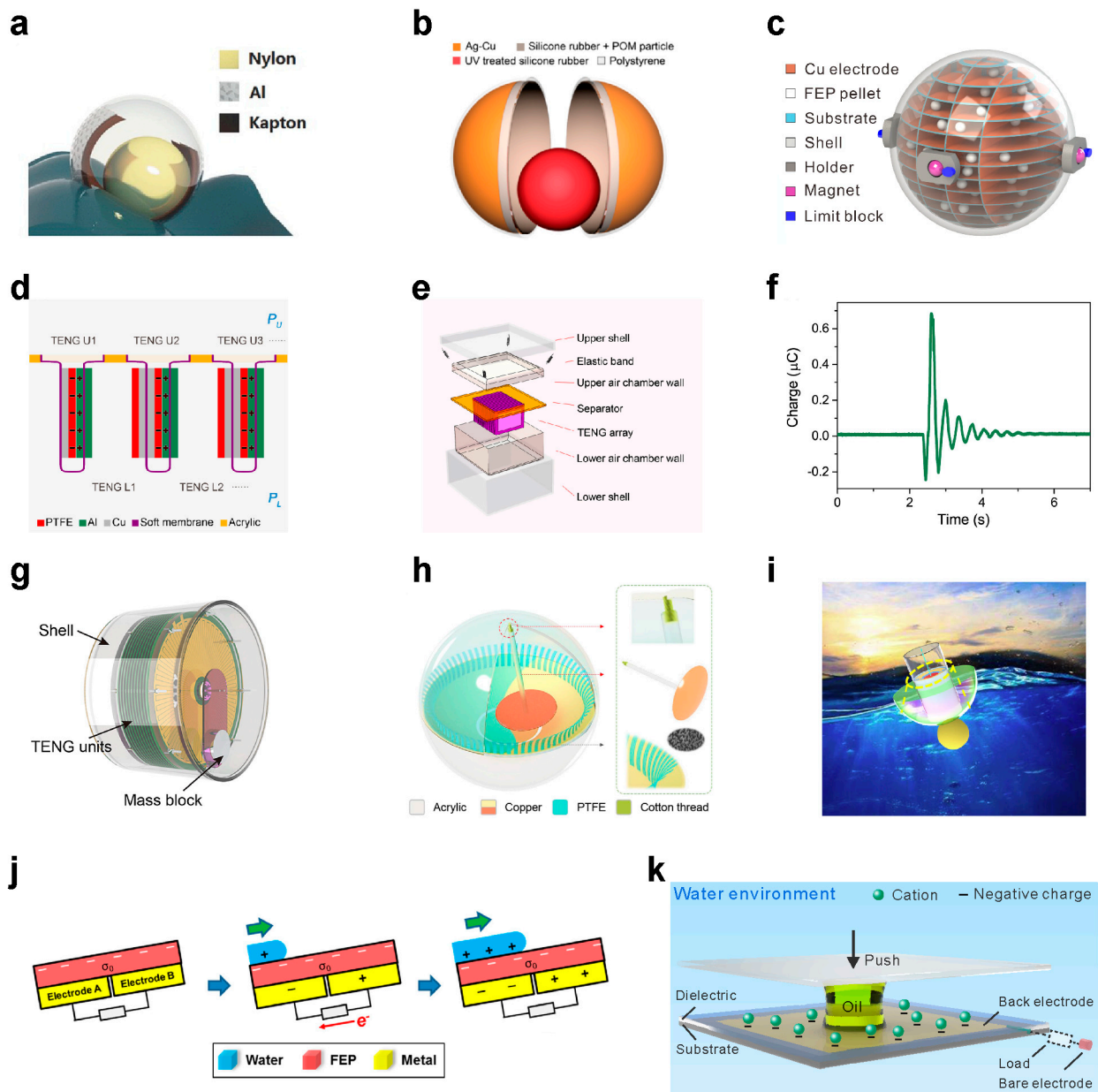


Figure 3. Schematics of typical TENG units. (a) A schematic diagram of the first rolling ball structure device based on the free-standing mode. Reprinted with permission from Ref. [23], copyright 2015, Wiley. (b) A schematic diagram of the rolling ball structure TENG unit using silicone rubber. Reprinted with permission from Ref. [24], copyright 2018, American Chemical Society. (c) A schematic structure of the three-dimensional electrode device. Reprinted with permission from Ref. [25], copyright 2019, Elsevier. (d) A schematic diagram of the multilayer structure in the TENG unit. (e) A schematic diagram of the spring-oscillator device design. (f) Oscillating output of the device after an impact agitation. (d–f) Reprinted with permission from Ref. [26], copyright 2016, Elsevier. (g) A schematic diagram of the device with the pendulum and grating structure. Reprinted with permission from Ref. [27], copyright 2019, Elsevier. (h) A schematic diagram of the device with the pendulum structure and soft contact. Reprinted with permission from Ref. [28], copyright 2019, Elsevier. (i) The device design with a combination of the pendulum and multilayer structure. Reprinted with permission from Ref. [29], copyright 2021, Elsevier. (j) Working mechanism of a typical liquid-solid contact structure. Reprinted with permission from Ref. [30], copyright 2014, American Chemical Society. (k) Structure of the device by sweeping out the charges in the electric double layer with oil. Reprinted with permission from Ref. [31], copyright 2022, Wiley.

3. Mechanical Connection

3.1. Simple Aggregation with Weak Coupling

Simple aggregation with weak coupling is the simplest form of networking structures, where units are either not connected or connected by strings, typically. In weakly coupled networks, mechanical connections primarily serve to fix the relative positions of the units within the network, with minimal interaction between units.

Chen et al. proposed a small-scale network woven from four units [32]. As shown in Figure 4a, each unit consists of four arch-shaped sub-units based on the contact-separation mode and a freely moving mass ball. Under water wave agitations, the ball collides with the sub-units, creating contact between the surfaces of the device. After the collision, separation occurs under the elasticity of the arch-shaped plates, generating AC outputs in the external circuit. The network composed of four units, as shown in Figure 4b, exhibits a nearly proportional relationship between the total rectified charge output and the number of units (Figure 4c). This indicates that the working state of the device is minimally affected by the weak coupling between the units in the simple aggregation network. Figure 4d illustrates the conceptual network based on a hierarchical architecture.

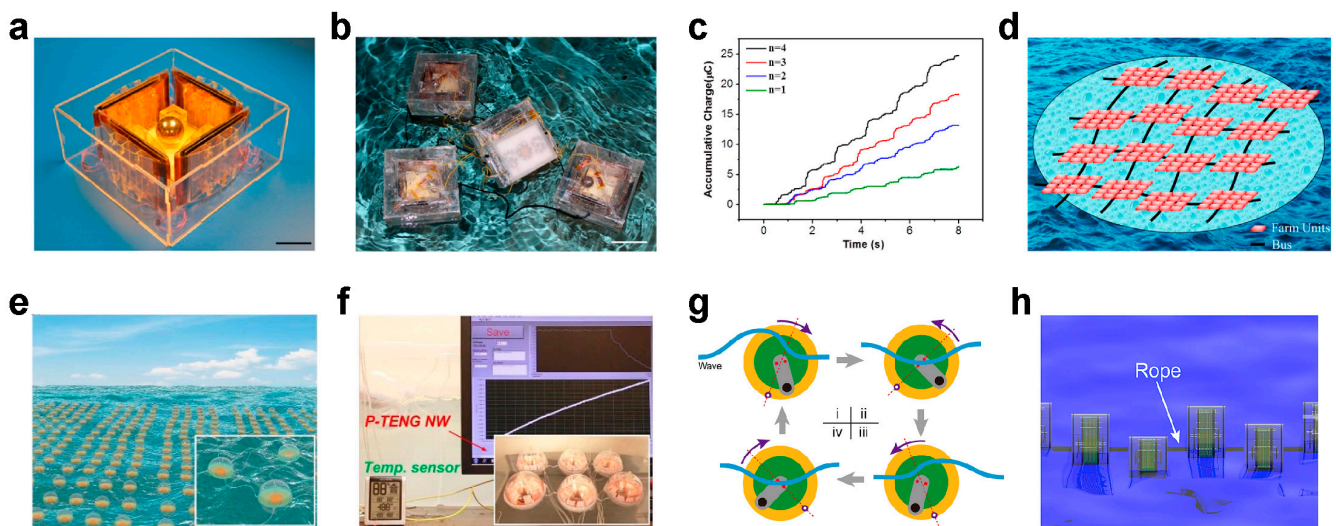


Figure 4. Networks in simple aggregation with weak coupling. (a) A photograph of the unit of the woven network. (b) A photograph of the woven network with 4 units. (c) The rectified charge output of different numbers of units. (d) A schematic diagram of the configuration of the hierarchical architecture network. (a–d) Reprinted with permission from Ref. [32], copyright 2015, American Chemical Society. (e) A schematic illustration of a large-scale network of pendulum structure TENGs. (f) A photograph of the TENG array to power a thermometer. (e,f) Reprinted with permission from Ref. [28], copyright 2019, Elsevier. (g) Working principle of the TENG in a string-connected network. (h) A schematic illustration of a string-connected network in water. (g,h) Reprinted with permission from Ref. [27], copyright 2019, Elsevier.

Lin et al. presented a network composed of pendulum structure units [28]. The unit structure is described above (Figure 3h), and a schematic diagram of a large-scale network composed of multiple units is shown in Figure 4e. In the water tank experiment, a 2×3 TENG array was constructed under simple aggregation as a power source for driving a thermometer. The 2×3 TENG array charged a $100 \mu\text{F}$ capacitor from 0 V to 3.1 V, achieving self-powered temperature sensing in 780 s (Figure 4f).

Bai et al. designed a string-connected network structure of a compound device with pendulum and multilayer structures [27]. The unit structure of this device is detailed in Figure 3g. The agitation process of the units in the network is illustrated in Figure 4g. The device is constrained from the bottom with ropes, allowing for rotation around the connection point. When subjected to water wave excitation, the mass block freely swings

together with the rotator, and the stator and shell move around the bottom connection point. After that, the device swings back under the influence of buoyancy and adjacent waves. The ropes connecting the units are under tension (Figure 4h), serving to fix the relative positions of the devices and anchor them.

3.2. Strongly Coupled Networks

A strongly coupled network is a networking strategy that enhances interactions between units in the network, typically using elastic connection structures. Characterized by its constraint effect, energy transfer, and cooperative effect, the strongly coupled network improves the output performance of units, which represents a large-scale, high-performance networking strategy of TENGs for harvesting blue energy.

Xu et al. conducted a detailed investigation into strongly coupled networks [24]. The units of the network adopt a rolling ball structure based on silicon rubber, as shown in Figure 3b. The impact of the network constraint effect on units was first studied (Figure 5a). For a specific unit's structure, there often exists a unit orientation most sensitive to external agitation, while in incorrect orientations, the unit exhibits extremely low or no outputs. In a real water wave environment, free unit orientations continuously change. The mechanical structure among units can impose a constraint effect, keeping units in proper orientation and anchoring their relative positions. The charging rate for the capacitor of a constraint unit is more than ten times of that of a free unit (Figure 5b).

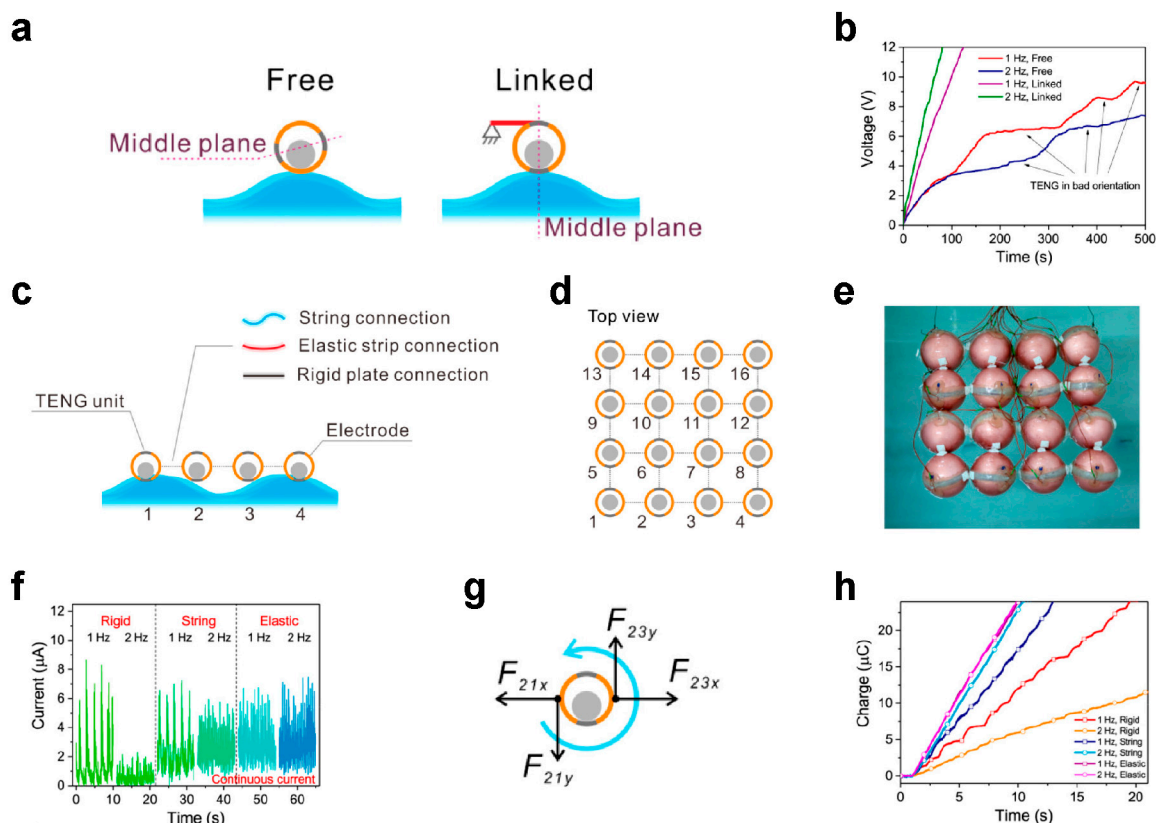


Figure 5. Strongly coupled network design and output performance. (a) A contrast schematic illustration of the TENG units in free and constrained states in water. (b) The performance of charging a capacitor of free and constrained units. (c) Schematics of three types of network connection. (d) Schematics of the networking structure. (e) A photograph of the connected network. (f) Rectified short-circuit current output of networks with different connections. (g) A schematic diagram of the force on a unit in the elastic connection network. (h) Rectified transferred charges of three different types of networks. (a–h) Reprinted with permission from Ref. [24], copyright 2018, American Chemical Society.

Moreover, three types of connections were tested, including rigid, string, and elastic connections (Figure 5c). Figure 5d shows the schematic illustration of the network of 16 TENG units arranged in a 4×4 array. The rigid connection creates a rigid body network without elasticity. Additionally, because of its ultra-soft property, the string connection only transmits tension force between units. The elastic type allows the transfer of elastic force within the network, typically using elastic strips for connection. The diverse force transmitted between units indicates the different local energy transfers of the networks. Fabricated networks, specifically as shown in Figure 5e, were tested in a water tank with water waves (Figure 5f). For a rigid network, the units synchronously move with strong constraints from rigid connections, outputting a high current peak at low frequency. However, the motions of a rigid network are inhibited when the wavelength and amplitude of waves decrease, resulting in extremely low output performance. The string and elastic connection networks exhibit similar current output characteristics with continuous and fluctuating parts, and the elastic connection network shows higher performance under different agitation frequencies. As a strongly coupled network, the elastic force and torque introduced by the elastic connection, together with the interaction force from the waves, can effectively agitate the unit in water waves (Figure 5g). Based on the cooperative effect of the units, it is even possible to achieve a resonance state between the network and the water waves. After rectification, the highest charge output rate of $2.7 \mu\text{C}$ per second was achieved by an elastic connection network at 2 Hz (Figure 5h).

Zhang et al. constructed a sea snake based TENG network with spring connections between the units [33]. The units of this network combine the rolling ball structure, multilayer structure, and spring-oscillator structure, which is composed of PTFE balls, nylon films, copper electrodes, and a tampered spring (Figure 6a). The curvature of the waves acts on the external acrylic shell, causing the unit to tilt to one side. The PTFE balls, influenced by their gravitational potential, roll towards the lower side. Simultaneously, the spring structure stores a portion of the energy and releases it while further driving the oscillation of the structure. A prototype of a sea snake structure network, consisting of three units connected through springs, is shown in Figure 6b. In a simulated wave environment, the impact of the number of network segments on device output is depicted in Figure 6c. The output voltage of a single-segment device is only 55 V. When the network expands to two and three segments, the output voltage increases to 160 V. This is due to the introduction of spring elasticity between the units, enhancing the cooperative effect within the network. Agitated by water surface curvature, the inclination angle of the segments and the horizontal motion of the device are enhanced. However, simple spring structures may face issues of rust and damage in a marine environment, leading to a decrease in network durability.

Hu et al. proposed a hyper-elastic network of wheel-structured TENGs, as shown in Figure 6d [34]. The units are interconnected with an improved elastic connection structure based on a silicone plate with meshes (Figure 6e), exhibiting nonlinearity in their stress-strain behavior and allowing for large elastic stretching. In contrast to the traditional smooth shells of devices, blade structures are added on the surface of the shell, enhancing the interaction between units and waves. This design allows the device to roll on the water surface like a wheel, agitating the internal TENG to output electrical energy (Figure 6f). The blade structure combined with the elastic connection structure, which stores and releases wave energy, enables efficient wave energy harvesting. Figure 6g–i illustrate three excitation modes of the network. Firstly, with an imbalanced force applied by waves or wind from one side, the rectangular frame of the unit moves translationally, inducing the shell with blades to roll on the water surface, while the orientation of the internal rotator remains nearly unchanged due to the gravitational force of the mass block (Figure 6g). Secondly, with the wave agitation between units, the elastic connection structure undergoes stretching and shrinking, driving the relative movement of the rectangular frames and causing the shells to roll (Figure 6h). Finally, under wave impacts, the swinging of the mass block inside the unit can also generate relative movements between the stator and the

rotator, resulting in electrical outputs (Figure 6i). In simulated waves, with a load resistance of 5 M Ω , the peak power and average power of two units are 1.125 mW and 0.1612 mW, respectively (Figure 6j).

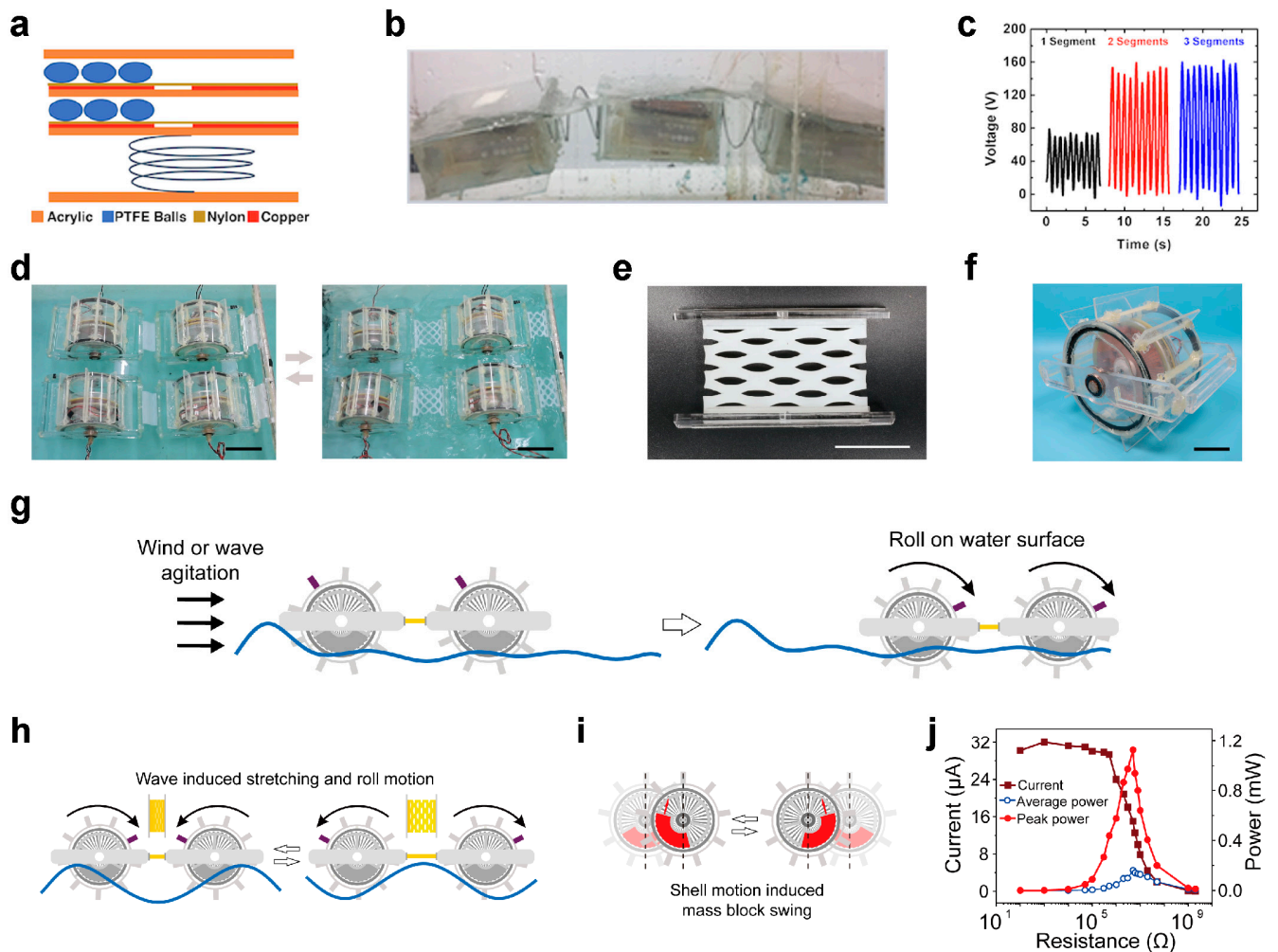


Figure 6. Strongly coupled network designs and output performance. (a) A schematic illustration of the unit in the sea snake TENG network. (b) A photograph of the 3-segment sea snake network in water. (c) The influence of the number of segments in the network on the voltage output of one unit. (a–c) Reprinted with permission from Ref. [33], copyright 2018, Elsevier. (d) Photographs of the hyper-elastic network of wheel-structured TENGs working in water. (e) A photograph of the connection structure in the stretched state. (f) A photograph of the wheel-structured TENG. (g) Directional roll motion of the units driven by waves or wind. (h) Roll motion of the units induced by the stretching and shrinking of the connection structure in water waves. (i) Swing motion of the inner mass block induced by waves. (j) Peak current, peak power, and average power of two networked units under various resistive loads. (d–j) Reprinted with permission from Ref. [34], copyright 2023, Wiley.

3.3. Dynamic Self-Assembly Networks

In a harsh marine environment, enhancing the mechanical robustness of network connections and maintaining the operational state of the network are critical challenges underlying network applications. The dynamic self-assembly networking strategy offers a viable solution to this issue, showcasing self-assembly behavior during the construction of the device network and self-healing behavior after network disconnection in extreme environments, which represent autonomy and mechanical robustness.

Yang et al. constructed a dynamic self-assembly network based on the connection structure of self-adaptive magnetic joints (SAM joints), as shown in Figure 7a,b [25]. The

SAM joint contains a well-confined magnetic ball structure. When the joints approach each other, the magnetic poles align automatically with the ball rotation and attract to connect. The design of a limit block restricts joint degrees of freedom, maintaining the network configuration in the horizontal plane while allowing for wave agitation in the vertical direction. As shown in Figure 7c–e, different numbers and positions of joints on the unit can achieve self-assembly networks with various topological structures, such as a hexagonal grid structure corresponding to three joints (Figure 7c), a square grid structure formed by four joints (Figure 7d), and a close-packed structure with six joints (Figure 7e). In a simulated wave environment, a self-assembly network containing 16 four-joint units was constructed (Figure 7f). Under wave agitation, this network successfully demonstrated self-healing behavior after being ruptured (Figure 7g). A network consisting of 18 TENG units could generate a rectified current of 35 μA . At a matching resistance of approximately 50 $\text{M}\Omega$, the peak power and average power were 34.6 mW and 9.89 mW, respectively. While dynamic self-assembly networks only focus on the mechanical connections of the network, the electrical connection between units requires further research.

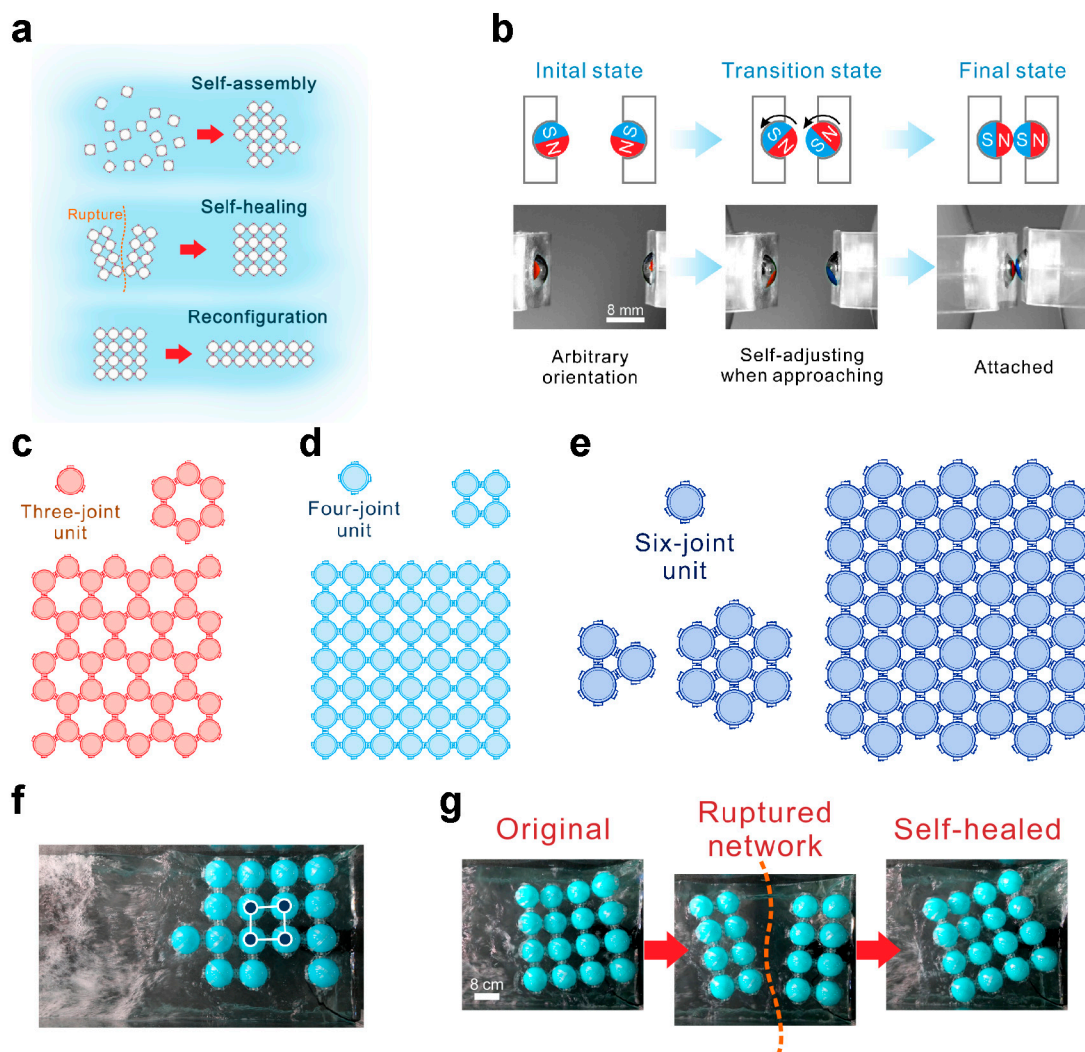


Figure 7. Dynamic self-assembly network design and behavior. (a) A schematic diagram of dynamic self-assembly network behavior. (b) The working mechanism of the self-adaptive magnetic joints (without the limit block). Schematic diagrams of the self-assembly networks for (c) three-joint units, (d) four-joint units, and (e) six-joint units. (f) A photograph of a network for four-joint units in water waves. (g) Self-healing process of the dynamic self-assembly network in water. (a–g) Reprinted with permission from Ref. [25], copyright 2019, Elsevier.

3.4. Chiral Networks

Chiral networks are a type of network based on chiral connection structures between units. Chiral connections break the symmetry of connections between units, and the asymmetric connection structure converts the interaction forces between units into torques acting on the units, causing units to rotate, which matches the excitation modes of most high-performance units. Chiral connection structures can use elastic materials to store energy, driving the units in reciprocal oscillation. The unique agitation mechanism of chiral networks can be further combined with other mechanical principles to achieve efficient harvesting of blue energy.

Wang et al. proposed a chiral network structure based on the contact-separation mode of TENGs (Figure 8a) [35]. In this design, the units are connected to each other through a pair of elastic rods fixed at the top and bottom of the shells, respectively. With wave excitation, the force on the bending elastic rods imposes a torque at the shell, causing the units to tilt. During the recovery process of the elastic rods, a torque in the opposite direction is generated, driving the units to tilt in the opposite direction. During the reciprocal tilting process, the slider can move relative to the stator in the direction perpendicular to the contact surface to achieve the contact-separation motion of the device.

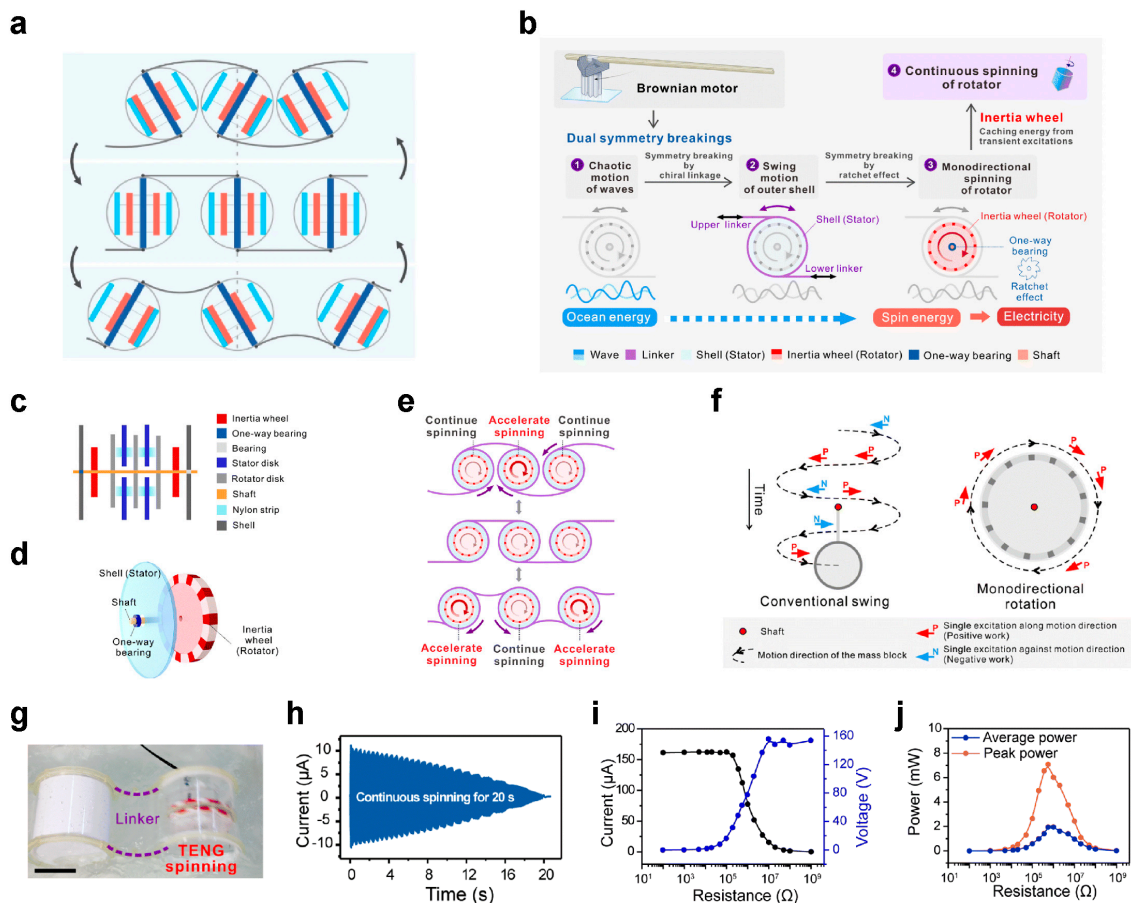


Figure 8. Chiral network design and performance. (a) Working principle of chiral network units in water. Reprinted with permission from Ref. [35], copyright 2020, the authors. (b) A schematic illustration of the general concept of the dual-symmetry-breaking system. (c) A schematic diagram of the unit structure. (d) A schematic diagram of the one-way bearing and inertia wheel structure. (e) Working principle of networked units in chiral linkage under wave excitations. (f) A schematic diagram of the monodirectional rotation. (g) Working state of the network in water. (h) Typical continuous short-circuit output after multiple excitations. (i) Peak current and load voltage of the unit with various loads in water. (j) Peak power and average power of the unit with different loads in water. (b–j) Reprinted with permission from Ref. [36], copyright 2023, Royal Society of Chemistry.

Inspired by microscale molecular systems, Qiu et al. introduced a design where chiral networks and one-way bearings were combined into a dual-symmetry-breaking structure [36]. This configuration transforms irregular, gentle wave excitations into monodirectional motion within the device. The working principle of this system is illustrated in Figure 8b, drawing inspiration from microscale Brownian motors, which can effectively extract energy in a chaotic environment through symmetry breaking. With the chiral connection, external random agitations are converted into swing motions of the outer shell. Then, through the one-way bearing with the ratchet effect, the shell's oscillation is converted into a monodirectional rotation of the internal rotator. Combined with the energy caching of the inertia wheel structure, this setup achieves the superposition of multiple excitations, resulting in a continuous spinning of the rotator. The unit's structure is depicted in Figure 8c, where the stator disks are fixed to the shell, and the rotating structure, consisting of the rotator disks, inertia wheel, and a shaft, is mounted inside the shell with bearings, including a one-way bearing. To reduce friction during relative rotation, a gap is introduced between the rotator disk and the stator disk. Triboelectric charges are generated through a nylon strip fixed at one end to the stator disk. The schematic diagram of the one-way bearing and inertia wheel structure is shown in Figure 8d.

The schematic illustration of networked devices in chiral linkage under wave excitations is illustrated in Figure 8e. Under wave agitations, the positions of the units oscillate, and the chiral connections, due to their elasticity, switch between bending and recovering states, causing the units to swing back and forth, thereby triggering the monodirectional rotation of the internal rotator. Due to energy caching in the inertia wheel, monodirectional rotation continues and is accelerated by subsequent excitations. In contrast, swing structures commonly used for long-time response behavior after a single agitation cannot avoid some excitations opposing the movement direction of the mass block, bringing negative work to the system (Figure 8f). The unidirectionality achieved through motion rectification ensures that each excitation contributes positive work along the rotation direction of the mass block. This allows energy to accumulate rapidly in the rotator. The working state of the network in water is shown in Figure 8g, where the networked unit can generate a typical continuous short-circuit output for 20 s after multiple excitations (Figure 8h). The device containing 10 sub-units can produce relatively high peak current and voltage in low-frequency waves of 0.67 Hz, as shown in Figure 8i, corresponding to the peak power and average power of 7.07 mW and 1.95 mW, respectively, at a resistance of 560 k Ω (Figure 8j).

3.5. Three-Dimensional Networks

The three-dimensional (3D) network refers to a TENG network that extends from the water surface to a certain depth underwater, forming a 3D spatial structure. Through a well-thought-out design of units and connection structures, strong interactions between the 3D network and the water body can be realized, enabling the harvesting of wave energy not only from the water surface but also from a certain depth underwater.

Li et al. proposed a 3D chiral TENG network based on metamaterial structures [37]. The schematic diagram of the 3D network is illustrated in Figure 9a, consisting of floats, chiral units, and ligaments. The chiral units have a semi-spherical mass shell on one side, forming an unbalanced structure. The units are connected by ligaments along the vertical direction to create an asymmetric chiral chain extending underwater. The top-layer floats keep the network's position relative to the water surface. The distributed units within the network can achieve effective motion and energy transfer through chiral connections, transmitting local agitation to different parts of the network. The dynamic behavior of this network is similar to the response of chiral mechanical metamaterials to mechanical waves.

Under mechanical pull and push, the chiral metamaterial behaves flexing of ligaments and rotation of annulus nodes, converting translational agitation into internal unit rotations, as shown in Figure 9b. The 3D chiral TENG network behaves similarly. Specifically, the force-torque coupling of units in the 3D TENG network is depicted in Figure 9c. With

the unit center as the pole, two sets of forces acting on the unit apply torques in opposite directions. The gravity-buoyancy torque (T_{GB}) results from the offset of the action point of gravity due to the attached mass shell on the chiral unit. The drive torque (T_D) is generated by tension in the ligaments under wave excitation. As the drive torque changes with waves, the chiral units roll back and forth. During this process, part of the energy “dissipates” to generate electricity by TENG units. Figure 9d illustrates the rotation process of chiral units in the network under wave excitation. For clarity, the network is unfolded into a two-dimensional plane, neglecting horizontal ligaments. The corresponding network initial and tensile states in a water environment are shown in Figure 9e,f. Since gravity-buoyancy energy is a form of potential energy, the dynamic behavior of the chiral network in water is similar to a spring, regarded as a hydro-gravity spring with hyper-elasticity (Figure 9g,h).

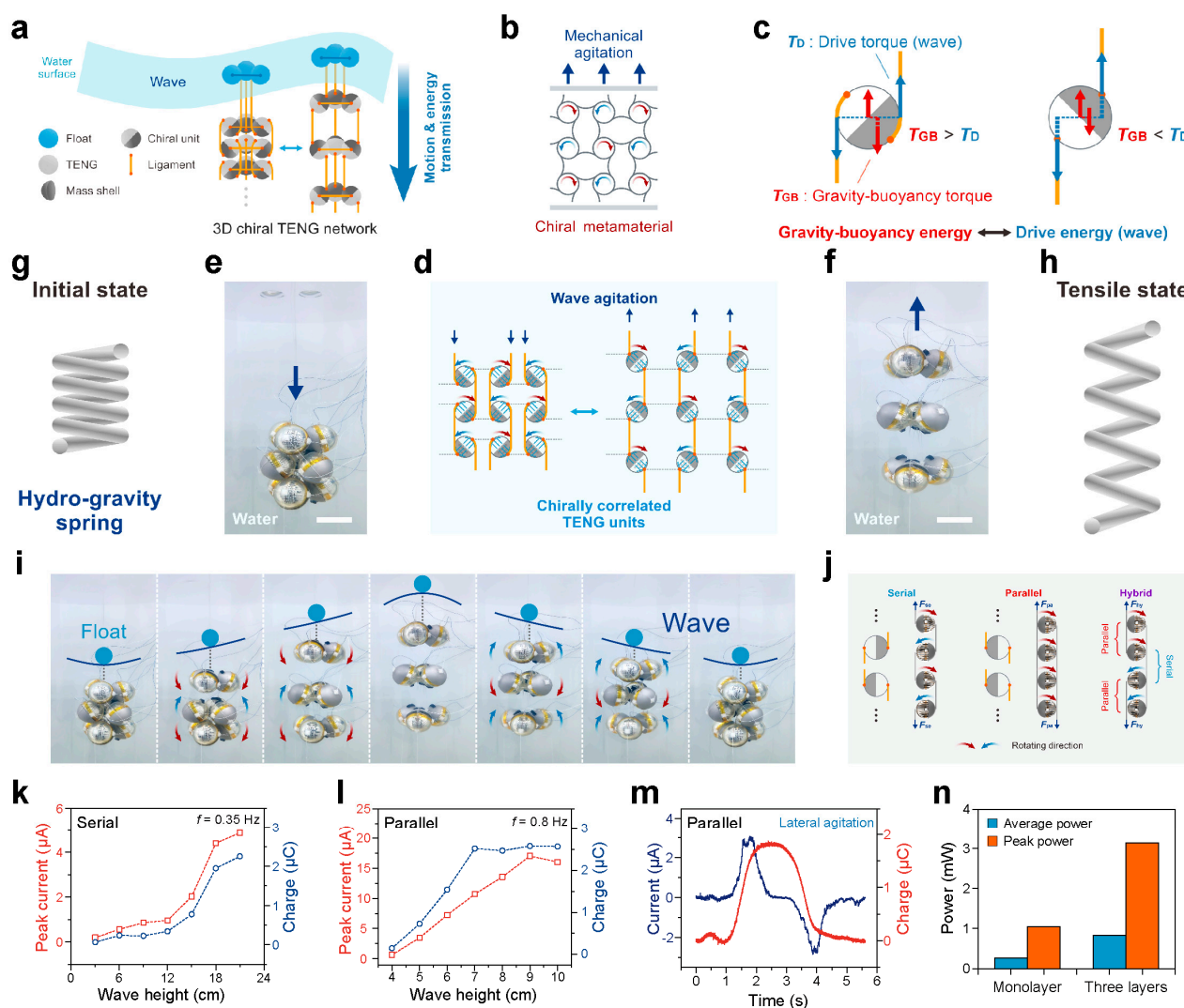


Figure 9. Three-dimensional network design and performance. (a) A schematic illustration of the 3D chiral TENG network. (b) A schematic diagram of the dynamic behavior of chiral metamaterials. (c) Force-torque coupling at a chiral unit. (d) Working mechanism of the 3D chiral TENG network. Photographs of the 3D chiral network in water with the (e) initial state and (f) tensile state. Schematics of an analogical hydro-gravity spring in the (g) initial state and (h) tensile state. (i) Motion process of the serial network under one-period wave agitation in water. (j) Serial, parallel, and hybrid types of chiral chains. Peak current and transferred charges of the (k) serial network and (l) parallel network. (m) Output of the parallel network under lateral agitation in one period. (n) Power comparison between monolayer and three-layer networks. (a–n) Reprinted with permission from Ref. [37], copyright 2023, Royal Society of Chemistry.

Figure 9i demonstrates the motion behavior of a chiral network composed of nine units under wave agitation. Within one wave period, the network unfolds and recovers like a spring. Moreover, the network has three connection forms: serial, parallel, and hybrid types (Figure 9j). Serial networks require smaller driving forces and larger driving distances, while parallel networks require larger driving forces and smaller driving distances, which were discussed in detail in the research. Hybrid networks are a combination of the two types. The relationship between the output of serial or parallel networks and wave height is shown in Figure 9k,l. The network also responds to underwater lateral agitation, with parallel networks producing a charge output of about $1.87 \mu\text{C}$ under a single lateral agitation (Figure 9m). As shown in Figure 9n, the extension of network layers roughly linearly enhances the power output of the network while maintaining the occupied sea area unchanged, representing an efficient strategy for harvesting wave energy.

4. Electrical Connection

4.1. Rectification and Power Management

Most TENG units output alternating current (AC), and the direction of the current depends on the motion state of the device, as shown in Figure 2b. When network units with asynchronous motions are directly electrically connected, current from the units can have opposite directions and cancel each other out, leading to decreased performances. Therefore, for asynchronous unit outputs in the network, rectification is performed separately for each unit before the electrical connection for a merged output (Figure 10a). After rectification, the AC output of the units is converted into direct current (DC). In this situation, the units are partly isolated, and the damage of one unit will not affect the output of the other units. For networks with synchronous motions, the units can be directly electrically connected to form the total output before the rectification, reducing cost and complexity. However, this increases the impact of damage of a single unit without the isolation effect provided by independent rectification (Figure 10a). The electrical output of TENG units has a relatively high voltage and low current. Parallel connections are usually adopted for the units in the network to increase the output current. Power management circuits are usually adopted to further tune the output, which can lower the voltage, enhance the current, and address the impedance mismatch between the high impedance of the TENG network and the low impedance of the application devices.

A typical schematic diagram of an electrical connection for an asynchronous unit output network is shown in Figure 10b, where 16 units in the network are rectified separately and connected in parallel [24]. The relationship between the total short-circuit current output and the number of units is depicted in Figure 10c, showing an approximately linear relationship between the peak current and the number of units. The superposed charge output is illustrated in Figure 10d, where the rectified charge output shows a one-sided growth trend due to rectification. Figure 10e,f show the output power of a single unit and a network consisting of 16 units, respectively, with different loads. Despite the variations in the test condition, it can be observed that through parallel electrical connections in the network, the output power multiplies, while the matching impedance is reduced several times, which is approximately equal to the number of units. Figure 10g presents an optimization design that utilizes the device's structure to keep partial sub-unit outputs synchronized, reducing the required number of rectification modules [36]. In Figure 10h, a parallel 3D network exhibits a synchronous motion of units under wave excitation, where units can be directly connected without the need for independent rectification [37]. Under a single-cycle agitation, the output of a non-rectified network is shown in Figure 10i.

Xi et al. demonstrated a power management circuit that incorporates a DC buck conversion module (Figure 10j) [38]. The switching function of the buck module is achieved through a voltage comparator and a MOSFET. Meanwhile, the switch has an additional effect to maximize the output energy within one cycle [13]. The released energy through the switch is tuned via the buck circuit and stored in the capacitor, powering the load. The power management circuit alters the matching impedance from $35 \text{ M}\Omega$ to $1 \text{ M}\Omega$ with low

energy loss at a frequency of 1 Hz, and its compact design allows for its application in various TENGs.

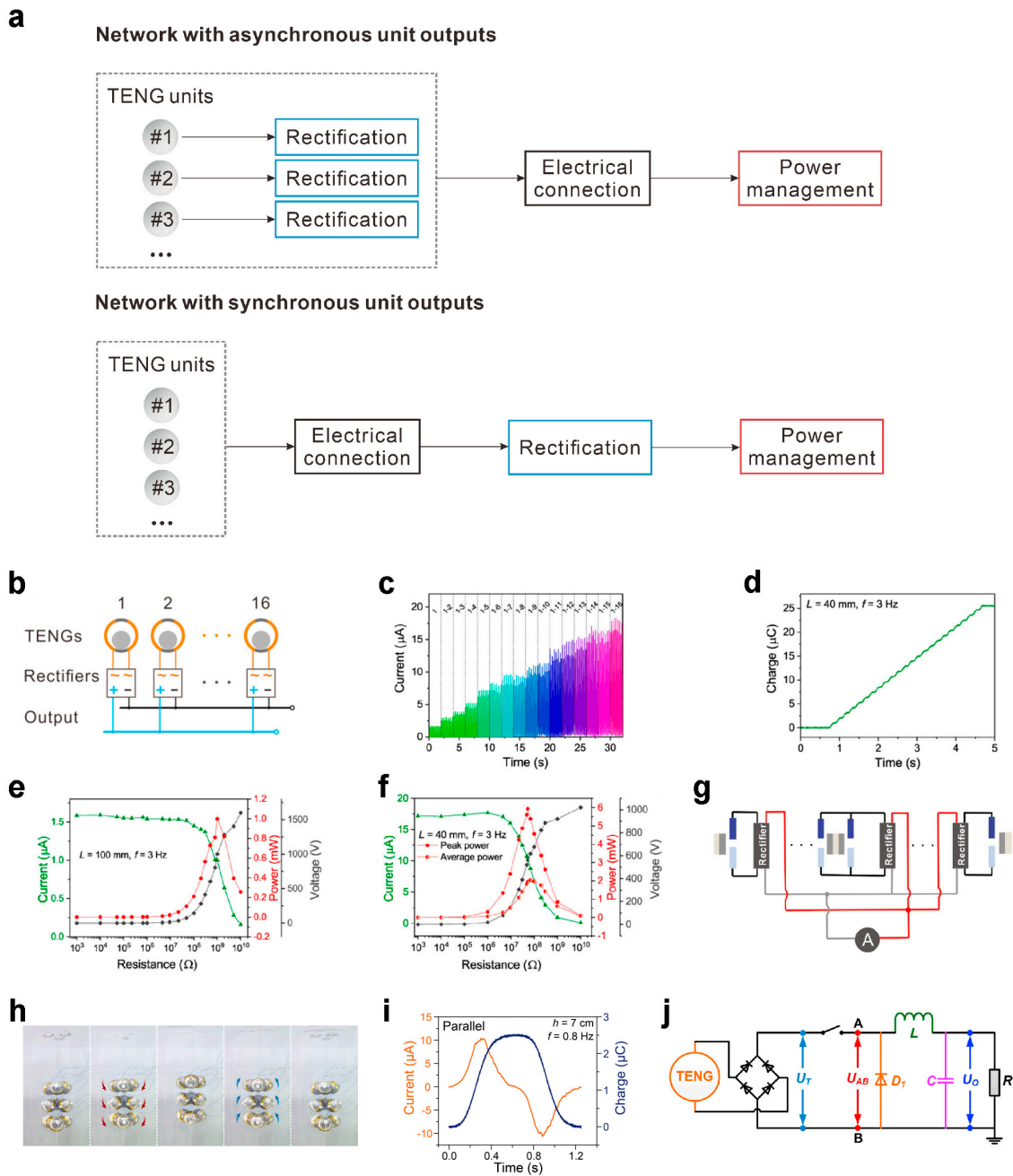


Figure 10. Rectification and power management of the network. (a) A schematic illustration of the network electrical connection. (b) A schematic diagram of separately rectified units connected in parallel. (c) Rectified short-circuit current with different amounts of units. (d) Charge output of the network with rectification. (e) Output power of a single unit with different loads. (f) Output power of a network consisting of 16 units with different loads. (b–f) Reprinted with permission from Ref. [24], copyright 2018, American Chemical Society. (g) A rectification circuit diagram of an optimized device. Reprinted with permission from Ref. [36], copyright 2023, Royal Society of Chemistry. (h) Motion process of the parallel 3D network under agitation in water. (i) Short-circuit current and transferred charges of the parallel 3D network under a single vertical agitation in water. (h,i) Reprinted with permission from Ref. [37], copyright 2023, Royal Society of Chemistry. (j) A schematic circuit diagram of the power management module. Reprinted with permission from Ref. [38], copyright 2017, Elsevier.

4.2. Networking Topology and Cable Loss

For the electrical connection and power transmission of TENG networks on a large scale, balancing cable loss and cable cost becomes important due to the significantly increased cable length. Liu et al. proposed four basic forms of network topology, which have different cable lengths, and studied the influence of cable impedance on network output, providing a theoretical foundation for the optimization of large-scale power networks [39].

The first electrical networking topology is illustrated in Figure 11a, where two adjacent TENG units are each connected through cables. Figure 11b depicts the lumped parameter model of the first networking topology. The second electrical networking topology is shown in Figure 11c, where all the TENG units are connected by cables at two points, and the lumped parameter model and simplified model are illustrated in Figure 11d. The calculation results indicate that the first networking topology structure leads to a significant decrease in the output power of the network. However, the number of cables used for the first networking topology is much fewer than those in the second topology, making it easier to deploy, integrate, and more cost-effective.

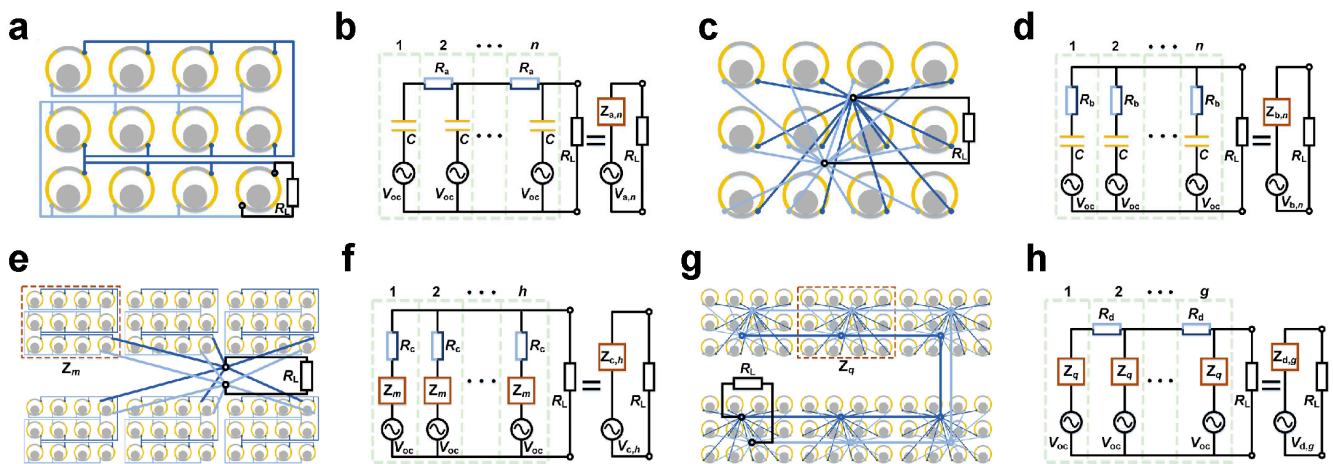


Figure 11. Electrical networking topology and circuit model. Schematics of the (a) first, (c) second, (e) third, and (g) fourth electrical networking topologies. Schematics of the lumped parameter model and simplified model of the (b) first, (d) second, (f) third, and (h) fourth electrical networking topologies. (a–h) Reprinted with permission from Ref. [39], copyright 2020, the authors.

To leverage the characteristics of the two topology structures, a third electrical networking topology with a hierarchical structure is proposed (Figure 11e), where the TENG network is divided into multiple modules, and each module includes multiple units. In each module, connections are made using the first networking topology, while connections between modules use the second network’s topology. Figure 11f shows the schematic diagrams of the lumped parameter model and simplified model. The fourth electrical networking topology, as shown in Figure 11g, has an alternate structure, with the connections within each module using the second networking topology and the connections between modules using the first network topology. The schematic diagrams of the lumped parameter model and simplified model are illustrated in Figure 11h. Computational results indicate that for networks containing the same number of units, adopting the third networking topology allows the TENG network to maintain a high transmission efficiency with relatively fewer cables. This is of significant importance for large-scale TENG networks, as the reduction in cable length can not only lower production costs but also reduce the complexity of TENG networks.

4.3. Multifunctional Design

Multifunctional design is an approach that extends the functions of cables beyond power transmission. Liu et al. proposed a cable design that not only transmits electrical

power but also acts as an energy harvester and mechanical connector [40]. Figure 12a illustrates a honeycomb-like network of flat power cables composed of spring steel tapes and three polymer films. The steel tapes inside the power cable serve dual purposes as the structural frame and electrodes. As depicted in Figure 12b, the cable is easily bent in the direction perpendicular to the plane, while it is hard to bend along the plane direction, ensuring the stability of the TENG network. Meanwhile, the steel tapes eliminate the influence of seawater on the output. The porous PTFE film on the outer side of the cable serves as a friction layer. When the water fluctuates around the power cable, friction charges can be generated on the surface (Figure 12c). As the shielding state of water changes, the induced charges move to balance the potential difference in the electrodes formed using the two steel tapes, enabling the cable itself to generate electricity. Figure 12d demonstrates the output signal generated through the periodic contact and separation of waves with the power cable. Furthermore, the hydrophobicity of the PTFE film is crucial for the output performance of the power cable (Figure 12e). Poor hydrophobicity results in residual water on the film, reducing the change in the shielding state and, consequently, decreasing the output. Using a single cable can achieve an open-circuit voltage of 34 V and transferred charges of 25 nC within a single cycle.

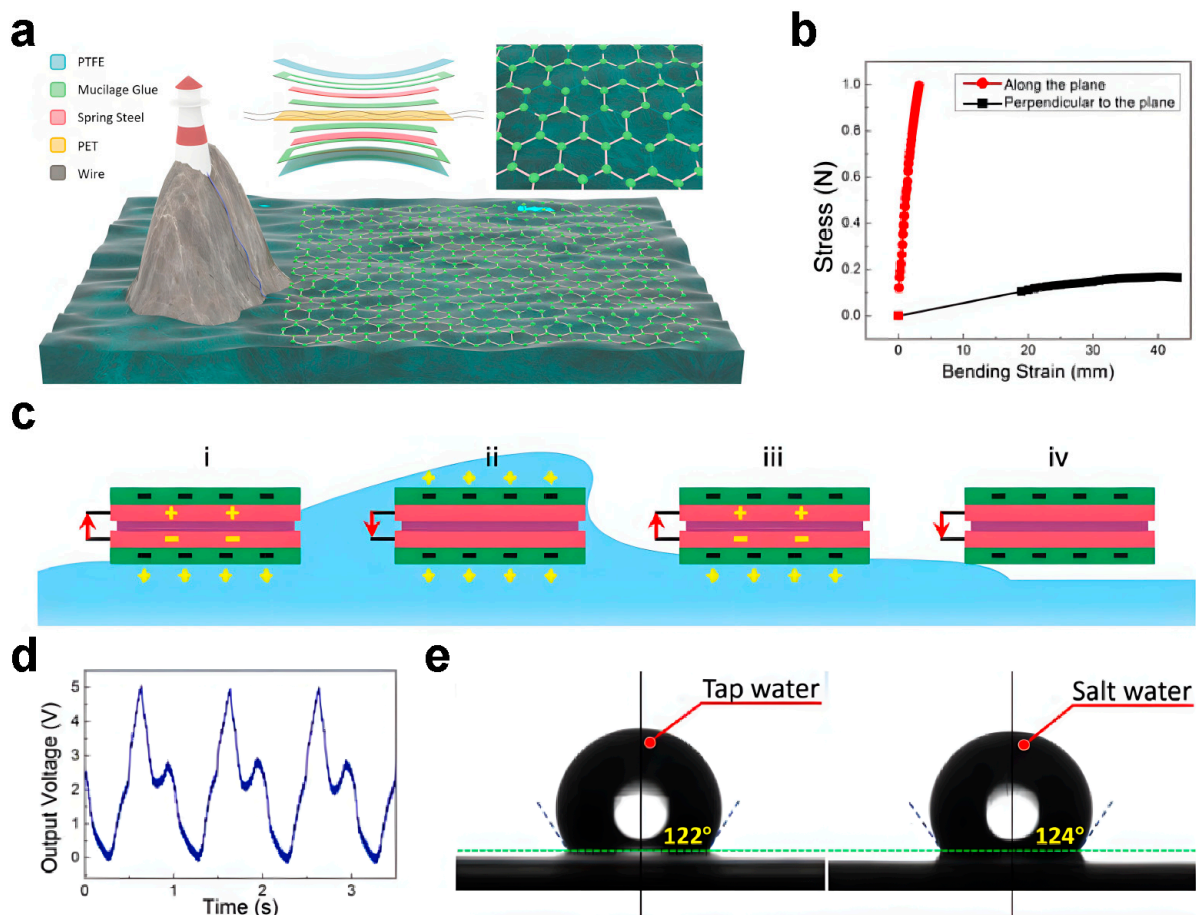


Figure 12. Multifunctional design and performance. (a) A schematic diagram of a multifunctional plane-like power cable. (b) Stress–strain curve of the power cable bending in two directions. (c) Working principle of the power cable under water agitation. (d) Output voltage of the power cable through periodic agitations. (e) Contact angle of tap water and salt water on the porous PTFE film. (a–e) Reprinted with permission from Ref. [40], copyright 2020, Elsevier.

5. Anchoring Strategy

5.1. Directly Anchoring to the Seabed

Anchoring is essential for ensuring the position of the devices in a harsh marine environment and should also adapt to the operational mode of the TENG. Directly connecting the units to the seabed is the simplest and most direct anchoring method, applicable for devices of various sizes and weights. However, the cost can be relatively high. In simulated wave environment experiments, a method of attaching the units directly to the wave tank wall is used for simulating the case.

The directly anchoring strategy has been applied in traditional wave energy harvesting equipment, and Figure 13a illustrates a typical design, which is called the Archimedes wave swing (AWS). The AWS is typically an air-filled cylinder immersed in water [41]. The cover of the air chamber can move vertically relative to the base fixed to the seabed. When the wave peak is above the AWS, the volume decreases due to the water pressure. Conversely, when the wave valley is above the AWS, the volume increases due to the internal air pressure. By altering the internal air pressure and volume of the AWS, the system frequency can be changed. When the system frequency matches the wave frequency, the linear motion's displacement can be much larger than the wave height. Energy is harvested from this process using a linear generator. Due to the specific working principle of the AWS, this device is directly anchored to the seabed to keep it submerged in water while maintaining the orientation of the device and the relative fixation of one end of the air chamber, which ensures that the AWS remains in its normal working state.

In a tower-like TENG unit proposed by Xu et al., PTFE balls roll between two electrodes, attached to a curved nylon film, to generate electricity, and the spatial utilization and output of the device are increased through a multilayer design (Figure 13b) [42]. In wave tank experiments, the unit's bottom is fixed to the tank bottom with a rope, simulating the effect of directly anchoring to the seabed in a real marine environment. Under the actions of waves, the unit swings, lighting up 540 LEDs (Figure 13c). Anchoring this device to a fixed point on the seabed through a rope keeps this device near the water surface, where wave energy is mainly distributed. Meanwhile, the anchoring rope can assist the device to swing under waves, effectively agitating the device, and its reasonable structural design can realize resonance with waves to enhance its output.

Sun et al. designed a bottom-fixed TENG for shore-based water wave energy [43]. Figure 13d shows the schematic diagram of the unit anchored at the coast, swinging and generating electricity under wave impact. This device mainly consists of two parts: two multilayer TENGs and an EMG unit with a coil, along with a sliding rail structure with an embedded permanent magnet (Figure 13e). The base and the device are connected using a spring, increasing the swing angle of the entire device. The capacitor charging performance under different connection modes was tested at an agitation frequency of 1.75 Hz, as shown in Figure 13f.

The drawstring TENG with modular electrodes proposed by Zhao et al. also adopts the strategy of anchoring directly to the seabed [44]. As shown in Figure 13g, the unit floats on the water surface and is anchored to the bottom with a drawstring. When the unit sways with the waves, the drawstring is pulled to agitate the device, which converts mechanical energy into electricity. The force analysis diagram of this device is shown in Figure 13h. The length of the drawstring is directly related to the wave parameters (Figure 13i). When the resonance frequency is equal to the wave frequency, the output can be maximized, as shown in the vibration mechanics model (Figure 13j). In a simulated wave environment, the variation in unit charge output with wave height at a frequency of 0.9 Hz is shown in Figure 13k, and the relationship between unit charge output and frequency under a wave height of 110 mm is shown in Figure 13l.

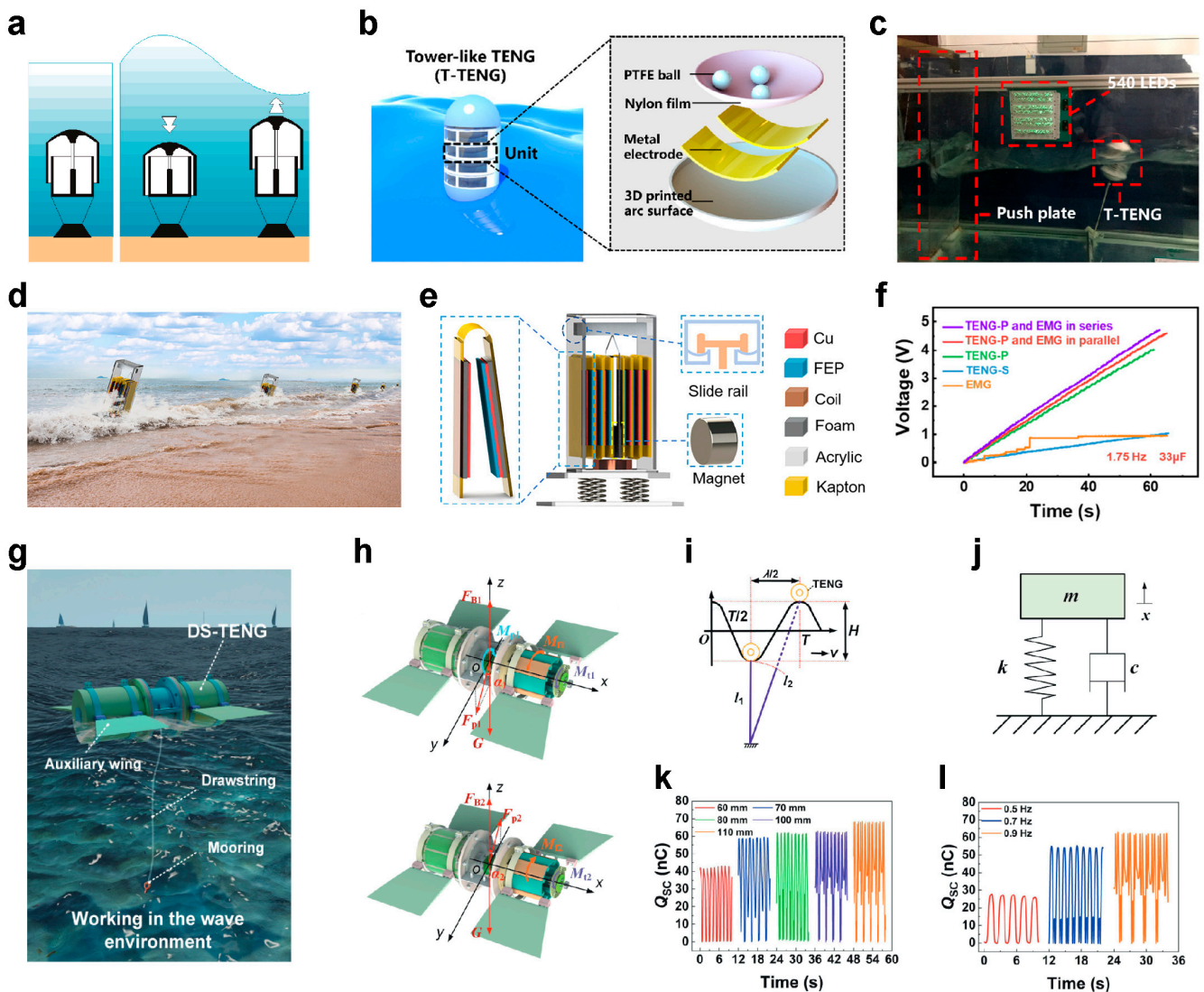


Figure 13. Directly anchoring to the seabed. (a) Working principle of the AWS in water. Reprinted with permission from Ref. [41], copyright 2005, Wiley. (b) A schematic diagram of a tower-like TENG unit structure. (c) A photograph of the tower-like TENG unit fixed to the tank bottom to power the LEDs. (b,c) Reprinted with permission from Ref. [42], copyright 2019, American Chemical Society. (d) A schematic diagram of the bottom-fixed units distributed along the shore to harvest water wave energy. (e) A schematic diagram of a bottom-fixed TENG unit structure. (f) Charging performance to capacitors under different connection modes. (d–f) Reprinted with permission from Ref. [43], copyright 2022, American Chemical Society. (g) A schematic illustration of the drawstring unit in the marine environment. (h) Force analysis diagram of the drawstring unit. (i) Motion state of the drawstring under wave agitation. (j) Vibration mechanics model of the unit. (k) Charge output at different wave heights with a frequency of 0.9 Hz. (l) Charge output at different frequencies under a wave height of 110 mm. (g–l) Reprinted with permission from Ref. [44], copyright 2023, Tsinghua University Press.

5.2. Attaching to Another Large Structure

Anchoring to another large structure, such as buoys anchored to the seabed, maritime vehicles, or other objects, serves as a more convenient anchoring method.

Xi et al. designed a TENG that adhered to a buoy structure [45]. The schematic illustration of the device is shown in Figure 14a, featuring a multilayer contact-separation structure and six sub-units. Each sub-unit utilizes a sponge as a buffer to attach two round FEP films to both sides of a mass. Cu films are chosen as the conductive layers, and

two springs are fixed on both sides of the mass. Driven by wave energy, assisted with the springs, the mass can vibrate and cyclically contact the top and bottom Cu films. In this process, alternating current is generated between the two copper electrodes. As shown in Figure 14b, TENG units are encapsulated in a small, waterproof cylindrical shell with the dimensions of $\Phi 15 \text{ cm} \times 7 \text{ cm}$. The sub-units of this device are connected in parallel and integrated into the buoy. A 2 Hz wave can drive the multilayer TENG to produce an open-circuit voltage of approximately 250 V and short-circuit transferred charges of 3 μC . This self-powered buoy system achieves signal transmission at 15 m in the 433 MHz frequency band, integrated with the power management module and monitoring module (Figure 14c).

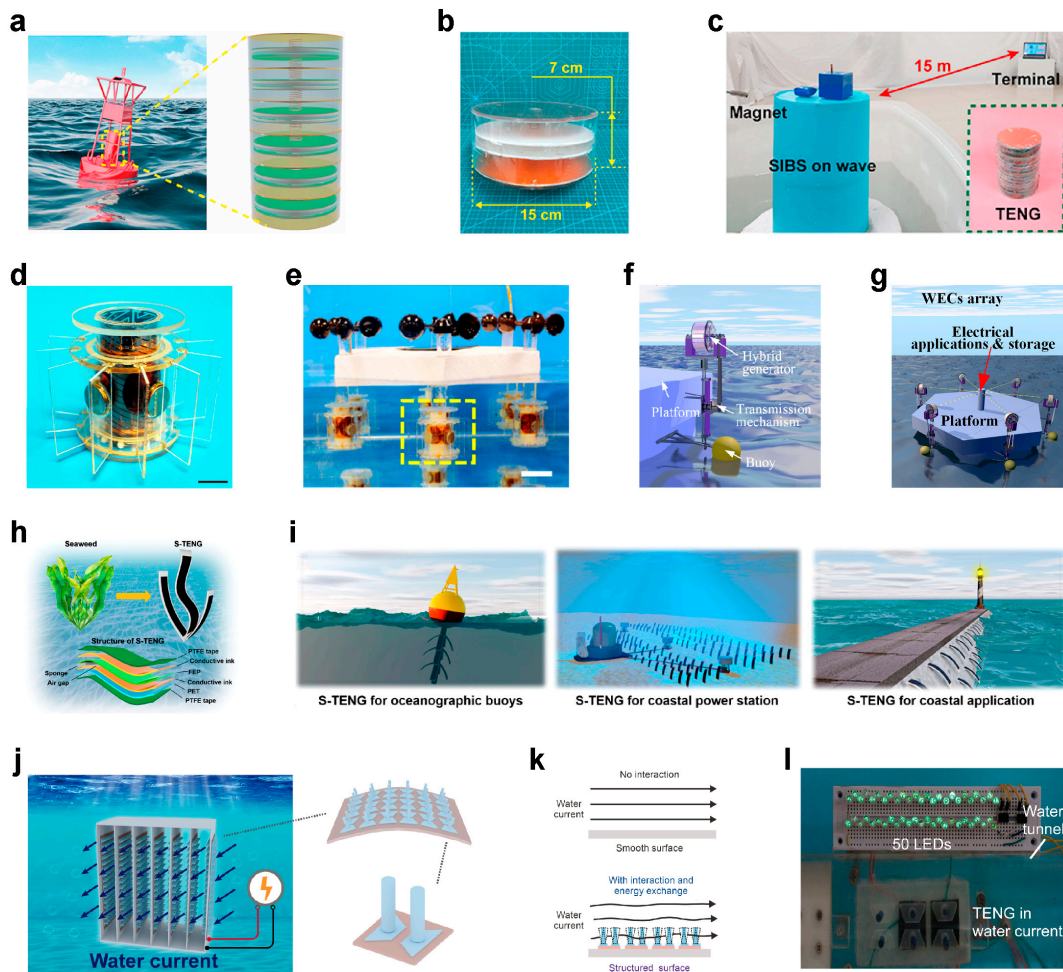


Figure 14. Attaching to another large structure. (a) A schematic illustration of the device adhered to a buoy structure. (b) A photograph of a fabricated unit adhered to a buoy structure. (c) Demonstration of the self-powered buoy system in a simulated wave environment. (a–c) Reprinted with permission from Ref. [45], copyright 2019, Elsevier. (d) A photograph of the hybrid generator. (e) A demonstration of the hybrid generator attached to an offshore platform. (d,e) Reprinted with permission from Ref. [46], copyright 2016, American Chemical Society. (f) A schematic illustration of a heaving point absorber-based hybrid generator. (g) Demonstration of a device array adhering to an ocean floater. (f,g) Reprinted with permission from Ref. [47], copyright 2021, Elsevier. (h) A schematic diagram of a flexible seaweed-like TENG. (h,i) Reprinted with permission from Ref. [48], copyright 2021, American Chemical Society. (j) A schematic illustration of the structured triboelectric surface (STS) for harvesting water current energy. (k) Comparison of water flowing through the smooth surface and STS. (l) A photograph of 50 LEDs lit up using the STS module. (j–l) Reprinted with permission from Ref. [49], copyright 2022, Wiley.

Wen et al. proposed a hybrid generator attached to an offshore platform [46]. This device consists of a spiral interdigital electrode TENG and a wrap-around EMG, containing three coaxially arranged cylindrical tubes. The outermost tube with adhered blades is responsive to water flow, enabling the device to operate in rotation and oscillation modes. The photograph of the as-fabricated device is shown in Figure 14d, and an anchoring scheme of attaching to a floating energy harvesting platform is proposed to collect different types of renewable energy (Figure 14e).

Zhao et al. designed a heaving point absorber-based hybrid generator adhered to a large platform, including a heaving buoy, a transmission mechanism, and an encapsulated magnetic coupling triboelectric-electromagnetic hybrid generator (Figure 14f) [47]. This hybrid generator consists of a multilayer soft-brush cylindrical TENG and a rotary disk EMG. The relative heaving motion of the buoy driven by wave energy is converted into unidirectional rotation of the rotator through a transmission mechanism, generating electricity. A device array based on the platform is also demonstrated, as shown in Figure 14g.

Inspired by seaweed structures, Wang et al. designed a flexible seaweed-like TENG that can attach to various surfaces [48]. The structural schematic illustration of this device is shown in Figure 14h, comprising a layer of FEP coated with conductive ink, a conductive ink-coated polyethylene terephthalate (PET) film, and two PTFE films. The friction layers are sealed within the PTFE layers to prevent contact with water. When the device periodically vibrates under excitation, the FEP film contacts and separates from the PET film cyclically, converting mechanical energy into electricity. Due to its flexibility, the device can attach to various structures, making it suitable for different marine applications, such as floating buoys, coastal power stations, and breakwaters, as shown in Figure 14i.

Deng et al. designed a flexible, structured triboelectric surface (STS) that can be attached to various structures for harvesting water current energy [49]. The basic concept of this device is shown in Figure 14j. The STS is a flexible structure composed of small arrayed TENG cells with outreaching pillars. Based on the vortex-induced vibration (VIV) principle and rigid-flexible coupling deformation structure, this device can effectively achieve contact separation under the agitation of water current. Figure 14k shows that, in contrast to a smooth surface, the surface structure of the STS can interact effectively with water current, transferring energy to the TENG array for power generation. Figure 14l demonstrates that under the agitation of water current, a small modular STS attached to the inner wall of a water tube can light up 50 LEDs. Due to its flexibility and modular design, it can be expanded into arrays of different scales and attached to different structures according to the requirements, demonstrating its great potential for various applications.

5.3. Anchoring as a Part of a Network

Connecting to the network can also be regarded as an anchoring strategy for units. As integral parts of the network, the units are subjected to the constraint effect of mechanical connections, fixing their relative positions within the network and maintaining a specific device orientation. When a part of the network is anchored on the seabed, other units in the network are indirectly anchored.

In the network strategy proposed by Li et al. for a 3D chiral TENG network, the prospect of a large-scale network as a marine power station is illustrated in Figure 15a [37]. This TENG network consists of several sub-networks, and each sub-network comprises multiple tubular modules, with their ends anchored to the seabed in practical applications. The power management modules collecting energy from each sub-network can distribute power for various applications or transmit energy to the mainland or islands through cables. In the practical tubular module, adjacent layers have a 60° angle between them and are connected through modified ligament connections, as shown in Figure 15b. Each unit is well constrained in this configuration, and when folded, it ensures a more stable stacking state. In this network, the end of the tubular module should be constrained, which allows for effective stretching of the module under waves. The constraints can be realized by connecting to a large damper or to the seabed, which can also realize the anchoring of the

network (Figure 15c). As shown in Figure 15d, the output of the network with constrained ends is significantly better than that of the network with free ends, realizing transferred charges of approximately $2.14 \mu\text{C}$.

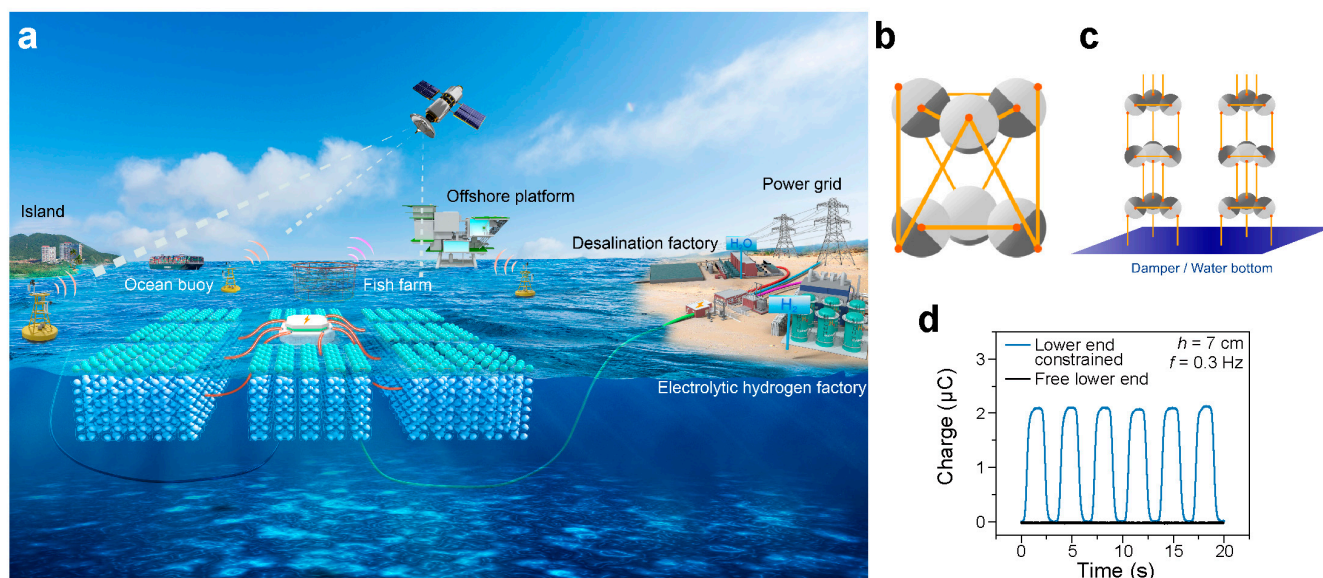


Figure 15. Anchoring as a part of a network. (a) The schematic prospect of a large-scale 3D chiral TENG network as a marine power station. (b) A schematic diagram of the practical network structure. (c) A schematic illustration of the 3D chiral TENG network with the lower end constrained. (d) Transferred charges of the network with different constraint states of the lower end. (a–d) Reprinted with permission from Ref. [37], copyright 2023, Royal Society of Chemistry.

6. Summary and Outlook

This paper provides a comprehensive overview of the networking strategies of TENGs for harvesting blue energy. The designs of mechanical and electrical connections of networks are mainly discussed, including simple aggregation with weak coupling, strongly coupled networks, dynamic self-assembly networks, chiral networks, three-dimensional networks for the mechanical connection and rectification and power management, networking topology and cable loss, and multifunctional design for the electrical connection. The anchoring strategies of devices and networks are also briefly discussed.

Diverse mechanical connections in the networks exhibit variations in the interactions among units and water waves, adapting to various networking requirements. In weakly coupled networks, the interaction among network units is minimal, and the units are almost independent. Strongly coupled networks, with the constraint effect, energy transfer, and cooperative effect, greatly enhance the interaction in the network. Dynamic self-assembly networks are designed to adapt to complex marine environments, featuring self-healing properties and reducing maintenance costs. Chiral networks convert wave excitation into an agitation torque acting on the units, and when combined with other mechanical mechanisms, the unit can achieve monodirectional continuous motion. Three-dimensional networks extend the network below the water surface, enabling the simultaneous harvesting of wave energy from all directions at a certain depth underwater, thereby enhancing energy utilization. The electrical connection should first consider the motion synchronization of network units and the requirement for rectification. The topology of electrical connections can be optimized to balance their cable losses and costs. Power management modules are also usually integrated to address the impedance mismatch between network outputs and application devices. The multifunctional design of cables can realize the functions of energy harvesting, mechanical connections, and electrical connections simultaneously. In further research, the following aspects can be focused on:

1. Designing units with higher power density is an essential approach to enhance the overall output of the network. In addition to advanced strategies, such as charge pumping [50], and optimizing the dielectric materials and structures of the units, the cooperative effect from networking should also be systematically investigated.
2. The interaction between water and units or networks significantly affects the energy utilization efficiency. Therefore, a comprehensive theoretical understanding based on fluid-structure interaction dynamics should be developed. Theoretical calculations should guide the design of units and networks.
3. The materials, connecting mechanisms, and topology of mechanical connections should be further optimized. The mechanical behavior from adjacent connected units to networks needs to be analyzed in detail. To better realize the relevant functions, such as maintaining the integrity of the network, improving the performance of single units, and enhancing the system efficiency of the network, new concepts and strategies need to be developed.
4. Designing high-efficiency electrical connection strategies that can transmit and merge the harvested power from distributed units is crucial, especially for large-scale networks that have relatively long cables. The connection should be cost-effective and minimize the influence from sea water. Meanwhile, the output also needs to be tuned using a power management circuit and distributed to different application devices that need to be studied in detail.
5. The mechanical and electrical connections in the network will undergo repeated deformation, which can suffer from fatigue issues. The durability of the connection structures must be well considered and improved in terms of materials and connecting mechanisms.
6. Given the complexity of real marine environments, corrosion and biofouling can be non-negligible problems for the connection structures in practical applications, which can be solved through adopting advanced materials and functional coatings.
7. The environmental friendliness of the network should also be emphasized. Minimizing the interference to the environment should be an important consideration in the design stage of the network.

Author Contributions: Conceptualization, L.X. and Z.L.W.; writing—original draft preparation, X.L.; writing—review and editing, L.X. and Z.L.W.; supervision, L.X. and Z.L.W.; project administration, L.X. and Z.L.W.; funding acquisition, Z.L.W. and L.X. All authors have read and agreed to the published version of the manuscript.

Funding: This work was supported by the Key Research Program of Frontier Sciences, CAS (grant no. ZDBS-LY-DQC025), the National Key R&D Project from the Minister of Science and Technology (2021YFA1201603 and 2021YFA1201601), the National Natural Science Foundation of China (51735001), and the Youth Innovation Promotion Association, CAS (2019170).

Data Availability Statement: No new data were created or analyzed in this study. Data sharing is not applicable to this article.

Conflicts of Interest: The authors declare no conflicts of interest.

References

1. Callaway, E. Energy: To Catch a Wave. *Nature* **2007**, *450*, 156–159. [[CrossRef](#)] [[PubMed](#)]
2. Scruggs, J.; Jacob, P. Harvesting Ocean Wave Energy. *Science* **2009**, *323*, 1176–1178. [[CrossRef](#)] [[PubMed](#)]
3. Isaacs, J.D.; Schmitt, W.R. Ocean Energy: Forms and Prospects. *Science* **1980**, *207*, 265–273. [[CrossRef](#)] [[PubMed](#)]
4. Chu, S.; Majumdar, A. Opportunities and Challenges for a Sustainable Energy Future. *Nature* **2012**, *488*, 294–303. [[CrossRef](#)] [[PubMed](#)]
5. Khaligh, A.; Onar, O.C. *Energy Harvesting: Solar, Wind, and Ocean Energy Conversion Systems*; CRC Press: Boca Raton, FL, USA, 2007; Volume 89.
6. Wang, Z.L.; Jiang, T.; Xu, L. Toward the Blue Energy Dream by Triboelectric Nanogenerator Networks. *Nano Energy* **2017**, *39*, 9–23. [[CrossRef](#)]
7. Falcao, A.F.D. Wave Energy Utilization: A Review of the Technologies. *Renew. Sust. Energy Rev.* **2010**, *14*, 899–918. [[CrossRef](#)]

8. Fan, F.-R.; Tian, Z.-Q.; Wang, Z.L. Flexible Triboelectric Generator. *Nano Energy* **2012**, *1*, 328–334. [[CrossRef](#)]
9. Wang, Z.L. Triboelectric Nanogenerators as New Energy Technology and Self-Powered Sensors—Principles, Problems and Perspectives. *Faraday Discuss.* **2014**, *176*, 447–458. [[CrossRef](#)]
10. Wang, Z.L.; Chen, J.; Lin, L. Progress in Triboelectric Nanogenerators as a New Energy Technology and Self-Powered Sensors. *Energy Environ. Sci.* **2015**, *8*, 2250–2282. [[CrossRef](#)]
11. Niu, S.; Wang, Z.L. Theoretical Systems of Triboelectric Nanogenerators. *Nano Energy* **2015**, *14*, 161–192. [[CrossRef](#)]
12. Wang, Z.L. On Maxwell's Displacement Current for Energy and Sensors: The Origin of Nanogenerators. *Mater. Today* **2017**, *20*, 74–82. [[CrossRef](#)]
13. Zi, Y.; Niu, S.; Wang, J.; Wen, Z.; Tang, W.; Wang, Z.L. Standards and Figure-of-Merits for Quantifying the Performance of Triboelectric Nanogenerators. *Nat. Commun.* **2015**, *6*, 8376. [[CrossRef](#)] [[PubMed](#)]
14. Wang, J.; Li, S.; Yi, F.; Zi, Y.; Lin, J.; Wang, X.; Xu, Y.; Wang, Z.L. Sustainably Powering Wearable Electronics Solely by Biomechanical Energy. *Nat. Commun.* **2016**, *7*, 12744. [[CrossRef](#)] [[PubMed](#)]
15. Bae, J.; Lee, J.; Kim, S.; Ha, J.; Lee, B.-S.; Park, Y.; Choong, C.; Kim, J.-B.; Wang, Z.L.; Kim, H.-Y.; et al. Flutter-Driven Triboelectrification for Harvesting Wind Energy. *Nat. Commun.* **2014**, *5*, 4929. [[CrossRef](#)] [[PubMed](#)]
16. Wang, Z.L. Catch Wave Power in Floating Nets. *Nature* **2017**, *542*, 159–160. [[CrossRef](#)]
17. Panda, S.; Hajra, S.; Oh, Y.; Oh, W.; Lee, J.; Shin, H.; Vivekananthan, V.; Yang, Y.; Mishra, Y.K.; Kim, H.J. Hybrid Nanogenerators for Ocean Energy Harvesting: Mechanisms, Designs, and Applications. *Small* **2023**, *19*, 2300847. [[CrossRef](#)]
18. Lin, L.; Xie, Y.; Niu, S.; Wang, S.; Yang, P.-K.; Wang, Z.L. Robust Triboelectric Nanogenerator Based on Rolling Electrification and Electrostatic Induction at an Instantaneous Energy Conversion Efficiency of ~55%. *ACS Nano* **2015**, *9*, 922–930. [[CrossRef](#)]
19. Niu, S.; Wang, S.; Lin, L.; Liu, Y.; Zhou, Y.S.; Hu, Y.; Wang, Z.L. Theoretical Study of Contact-Mode Triboelectric Nanogenerators as an Effective Power Source. *Energy Environ. Sci.* **2013**, *6*, 3576–3583. [[CrossRef](#)]
20. Niu, S.; Liu, Y.; Wang, S.; Lin, L.; Zhou, Y.S.; Hu, Y.; Wang, Z.L. Theory of Sliding-Mode Triboelectric Nanogenerators. *Adv. Mater.* **2013**, *25*, 6184–6193. [[CrossRef](#)]
21. Niu, S.; Liu, Y.; Wang, S.; Lin, L.; Zhou, Y.S.; Hu, Y.; Wang, Z.L. Theoretical Investigation and Structural Optimization of Single-Electrode Triboelectric Nanogenerators. *Adv. Funct. Mater.* **2014**, *24*, 3332–3340. [[CrossRef](#)]
22. Niu, S.; Liu, Y.; Chen, X.; Wang, S.; Zhou, Y.S.; Lin, L.; Xie, Y.; Wang, Z.L. Theory of Freestanding Triboelectric-Layer-Based Nanogenerators. *Nano Energy* **2015**, *12*, 760–774. [[CrossRef](#)]
23. Wang, X.; Niu, S.; Yin, Y.; Yi, F.; You, Z.; Wang, Z.L. Triboelectric Nanogenerator Based on Fully Enclosed Rolling Spherical Structure for Harvesting Low-Frequency Water Wave Energy. *Adv. Energy Mater.* **2015**, *5*, 1501467. [[CrossRef](#)]
24. Xu, L.; Jiang, T.; Lin, P.; Shao, J.J.; He, C.; Zhong, W.; Chen, X.Y.; Wang, Z.L. Coupled Triboelectric Nanogenerator Networks for Efficient Water Wave Energy Harvesting. *ACS Nano* **2018**, *12*, 1849–1858. [[CrossRef](#)]
25. Yang, X.; Xu, L.; Lin, P.; Zhong, W.; Bai, Y.; Luo, J.; Chen, J.; Wang, Z.L. Macroscopic Self-Assembly Network of Encapsulated High-Performance Triboelectric Nanogenerators for Water Wave Energy Harvesting. *Nano Energy* **2019**, *60*, 404–412. [[CrossRef](#)]
26. Xu, L.; Pang, Y.; Zhang, C.; Jiang, T.; Chen, X.; Luo, J.; Tang, W.; Cao, X.; Wang, Z.L. Integrated Triboelectric Nanogenerator Array Based on Air-Driven Membrane Structures for Water Wave Energy Harvesting. *Nano Energy* **2017**, *31*, 351–358. [[CrossRef](#)]
27. Bai, Y.; Xu, L.; He, C.; Zhu, L.; Yang, X.; Jiang, T.; Nie, J.; Zhong, W.; Wang, Z.L. High-Performance Triboelectric Nanogenerators for Self-Powered, in-Situ and Real-Time Water Quality Mapping. *Nano Energy* **2019**, *66*, 104117. [[CrossRef](#)]
28. Lin, Z.; Zhang, B.; Guo, H.; Wu, Z.; Zou, H.; Yang, J.; Wang, Z.L. Super-Robust and Frequency-Multiplied Triboelectric Nanogenerator for Efficient Harvesting Water and Wind Energy. *Nano Energy* **2019**, *64*, 103908. [[CrossRef](#)]
29. Zhang, C.; He, L.; Zhou, L.; Yang, O.; Yuan, W.; Wei, X.; Liu, Y.; Lu, L.; Wang, J.; Wang, Z.L. Active Resonance Triboelectric Nanogenerator for Harvesting Omnidirectional Water-Wave Energy. *Joule* **2021**, *5*, 1613–1623. [[CrossRef](#)]
30. Zhu, G.; Su, Y.; Bai, P.; Chen, J.; Jing, Q.; Yang, W.; Wang, Z.L. Harvesting Water Wave Energy by Asymmetric Screening of Electrostatic Charges on a Nanostructured Hydrophobic Thin-Film Surface. *ACS Nano* **2014**, *8*, 6031–6037. [[CrossRef](#)]
31. Qin, H.; Xu, L.; Lin, S.; Zhan, F.; Dong, K.; Han, K.; Wang, H.; Feng, Y.; Wang, Z.L. Underwater Energy Harvesting and Sensing by Sweeping Out the Charges in an Electric Double Layer Using an Oil Droplet. *Adv. Funct. Mater.* **2022**, *32*, 2111662. [[CrossRef](#)]
32. Chen, J.; Yang, J.; Li, Z.; Fan, X.; Zi, Y.; Jing, Q.; Guo, H.; Wen, Z.; Pradel, K.C.; Niu, S.; et al. Networks of Triboelectric Nanogenerators for Harvesting Water Wave Energy: A Potential Approach toward Blue Energy. *ACS Nano* **2015**, *9*, 3324–3331. [[CrossRef](#)]
33. Zhang, S.L.; Xu, M.; Zhang, C.; Wang, Y.-C.; Zou, H.; He, X.; Wang, Z.; Wang, Z.L. Rationally Designed Sea Snake Structure Based Triboelectric Nanogenerators for Effectively and Efficiently Harvesting Ocean Wave Energy with Minimized Water Screening Effect. *Nano Energy* **2018**, *48*, 421–429. [[CrossRef](#)]
34. Hu, Y.; Qiu, H.; Sun, Q.; Wang, Z.L.; Xu, L. Wheel-structured Triboelectric Nanogenerators with Hyperelastic Networking for High-Performance Wave Energy Harvesting. *Small Methods* **2023**, *7*, 2300582. [[CrossRef](#)] [[PubMed](#)]
35. Wang, H.; Xu, L.; Bai, Y.; Wang, Z.L. Pumping up the Charge Density of a Triboelectric Nanogenerator by Charge-Shuttling. *Nat. Commun.* **2020**, *11*, 4203. [[CrossRef](#)] [[PubMed](#)]
36. Qiu, H.; Wang, H.; Xu, L.; Zheng, M.; Wang, Z.L. Brownian Motor Inspired Monodirectional Continuous Spinning Triboelectric Nanogenerators for Extracting Energy from Irregular Gentle Water Waves. *Energy Environ. Sci.* **2023**, *16*, 473–483. [[CrossRef](#)]
37. Li, X.; Xu, L.; Lin, P.; Yang, X.; Wang, H.; Qin, H.; Wang, Z.L. Three-Dimensional Chiral Networks of Triboelectric Nanogenerators Inspired by Metamaterial's Structure. *Energy Environ. Sci.* **2023**, *16*, 3040–3052. [[CrossRef](#)]

38. Xi, F.; Pang, Y.; Li, W.; Jiang, T.; Zhang, L.; Guo, T.; Liu, G.; Zhang, C.; Wang, Z.L. Universal Power Management Strategy for Triboelectric Nanogenerator. *Nano Energy* **2017**, *37*, 168–176. [[CrossRef](#)]
39. Liu, W.; Xu, L.; Liu, G.; Yang, H.; Bu, T.; Fu, X.; Xu, S.; Fang, C.; Zhang, C. Network Topology Optimization of Triboelectric Nanogenerators for Effectively Harvesting Ocean Wave Energy. *iScience* **2020**, *23*, 101848. [[CrossRef](#)]
40. Liu, G.; Xiao, L.; Chen, C.; Liu, W.; Pu, X.; Wu, Z.; Hu, C.; Wang, Z.L. Power Cables for Triboelectric Nanogenerator Networks for Large-Scale Blue Energy Harvesting. *Nano Energy* **2020**, *75*, 104975. [[CrossRef](#)]
41. Polinder, H.; Damen, M.E.C.; Gardner, F. Design, Modelling and Test Results of the AWS PM Linear Generator. *Eur. Trans. Electr. Power* **2005**, *15*, 245–256. [[CrossRef](#)]
42. Xu, M.; Zhao, T.; Wang, C.; Zhang, S.L.; Li, Z.; Pan, X.; Wang, Z.L. High Power Density Tower-like Triboelectric Nanogenerator for Harvesting Arbitrary Directional Water Wave Energy. *ACS Nano* **2019**, *13*, 1932–1939. [[CrossRef](#)] [[PubMed](#)]
43. Sun, Y.; Zheng, F.; Wei, X.; Shi, Y.; Li, R.; Wang, B.; Wang, L.; Wu, Z.; Wang, Z.L. Pendular-Translational Hybrid Nanogenerator Harvesting Water Wave Energy. *ACS Appl. Mater. Interfaces* **2022**, *14*, 15187–15194. [[CrossRef](#)] [[PubMed](#)]
44. Zhao, D.; Li, H.; Wang, J.; Gao, Q.; Yu, Y.; Wen, J.; Wang, Z.L.; Cheng, T. A Drawstring Triboelectric Nanogenerator with Modular Electrodes for Harvesting Wave Energy. *Nano Res.* **2023**, *16*, 10931–10937. [[CrossRef](#)]
45. Xi, F.; Pang, Y.; Liu, G.; Wang, S.; Li, W.; Zhang, C.; Wang, Z.L. Self-Powered Intelligent Buoy System by Water Wave Energy for Sustainable and Autonomous Wireless Sensing and Data Transmission. *Nano Energy* **2019**, *61*, 1–9. [[CrossRef](#)]
46. Wen, Z.; Guo, H.; Zi, Y.; Yeh, M.-H.; Wang, X.; Deng, J.; Wang, J.; Li, S.; Hu, C.; Zhu, L.; et al. Harvesting Broad Frequency Band Blue Energy by a Triboelectric–Electromagnetic Hybrid Nanogenerator. *ACS Nano* **2016**, *10*, 6526–6534. [[CrossRef](#)] [[PubMed](#)]
47. Zhao, B.; Li, Z.; Liao, X.; Qiao, L.; Li, Y.; Dong, S.; Zhang, Z.; Zhang, B. A Heaving Point Absorber-Based Ocean Wave Energy Converter Hybridizing a Multilayered Soft-Brush Cylindrical Triboelectric Generator and an Electromagnetic Generator. *Nano Energy* **2021**, *89*, 106381. [[CrossRef](#)]
48. Wang, Y.; Liu, X.; Wang, Y.; Wang, H.; Zhang, S.L.; Zhao, T.; Xu, M.; Wang, Z.L. Flexible Seaweed-Like Triboelectric Nanogenerator as a Wave Energy Harvester Powering Marine Internet of Things. *ACS Nano* **2021**, *15*, 15700–15709. [[CrossRef](#)]
49. Deng, Z.; Xu, L.; Qin, H.; Li, X.; Duan, J.; Hou, B.; Wang, Z.L. Rationally Structured Triboelectric Nanogenerator Arrays for Harvesting Water-Current Energy and Self-Powered Sensing. *Adv. Mater.* **2022**, *34*, 2205064. [[CrossRef](#)]
50. Xu, L.; Bu, T.Z.; Yang, X.D.; Zhang, C.; Wang, Z.L. Ultrahigh Charge Density Realized by Charge Pumping at Ambient Conditions for Triboelectric Nanogenerators. *Nano Energy* **2018**, *49*, 625–633. [[CrossRef](#)]

Disclaimer/Publisher’s Note: The statements, opinions and data contained in all publications are solely those of the individual author(s) and contributor(s) and not of MDPI and/or the editor(s). MDPI and/or the editor(s) disclaim responsibility for any injury to people or property resulting from any ideas, methods, instructions or products referred to in the content.